The Thesis Committee for Ningjie Hu
Certifies that this is the approved version of the following thesis:

Lithofacies, Depositional Environment, and Stratigraphic Architecture of the Deep-Water Hybrid Mudrock System of the Pennsylvanian (Desmoinesian) Cherokee Group, Anadarko Basin, Texas Panhandle

APPROVED BY
SUPERVISING COMMITTEE:

Robert G. Loucks, Supervisor

Gregory Frébourg, Co-Supervisor

William L. Fisher

David Mohrig

Lithofacies, Depositional Environment, and Stratigraphic Architecture of the Deep-Water Hybrid Mudrock System of the Pennsylvanian (Desmoinesian) Cherokee Group, Western Anadarko Basin, Texas Panhandle

by

Ningjie Hu, B.S.

Thesis

Presented to the Faculty of the Graduate School of

The University of Texas at Austin

in Partial Fulfillment

of the Requirements

for the Degree of

Master of Science in Geological Sciences

The University of Texas at Austin

May, 2016

Dedication

To my parents who consistently offer me unconditional support and love

Acknowledgements

I would like to express my sincere thanks to my advisors Dr. Robert Loucks and Dr. Gregory Frébourg, for the guidance to formulate and address the research questions and for their generous support of this thesis. Bob, thank you for the knowledgeable, insightful and enjoyable discussions. Working with you has been a wonderful learning experience on both geology and life. I am grateful to Greg who give me such an incredible opportunity to study at the Jackson School of Geosciences and undertake this project. Thank you for the great discussions on sedimentology and always remind me of the importance of work-life balance. I would also like to thank my other committee members, Drs. William Fisher and David Mohrig, for their efforts to help me complete this project. Drs. Fisher and Mohrig are outstanding teacher and it was a great privilege and pleasure to take their classes. Dr. Mohrig gave very helpful advice to the data interpretation process for this thesis.

Special thanks to Bill Ambrose and Jacob Covault for the insightful discussion and extensive support to this project. Thanks also go to Bill Galloway, Stephen Ruppel, David Carr, Tucker Hentz, Rob Reed, Patrick Smith, Ray Eastwood, Harry Rowe, Evan Sivil, Nate Ivicic, and James Donnelly for providing their expertise and time to this project.

I appreciate STARR and Mudrock Systems Research Laboratory (MSRL) at the Bureau of Economic Geology, Jackson School of Geosciences, for finical support and providing a great platform to polish the research. Travel award was provided by AGU.

To my fellow MSRL students and officemates (Lauren Redmond, Chris Hendrix, and Kyle McKenzie), I appreciate sharing our graduate experience together and will miss your friendship, discussions, and company. I especially thank Lauren Redmond for sharing the challenging time and being very supportive. Thanks also go to Hang Deng, for being a

good listener and a cheerful friend. I appreciate all my friends who made my life happy and special at the Jackson School of Geosciences.

All of this would not have been possible without the support of my family. As the only child, I am very lucky to have loving and supportive parents who encouraged me to pursue my dream and study in the United States. My parents instilled in me an aspiration for knowledge and the courage to overcome the difficulties, taught me that the first priority in life is education which made me a better person. Their understanding, encouragement, and love were crucial in becoming who I am today. Thus, I dedicate my thesis to my parents, the most important people in my life.

Abstract

Lithofacies, Depositional Environment, and Stratigraphic Architecture of the Deep-Water Hybrid Mudrock System of the Pennsylvanian (Desmoinesian) Cherokee Group, Western Anadarko Basin, Texas Panhandle

Ningjie Hu, M.S. Geo. Sci.

The University of Texas at Austin, 2016

Supervisors: Robert G. Loucks and Gregory Frébourg

The Cherokee Group in the western Anadarko Basin, northeastern Texas Panhandle, is a Desmoinesian hybrid system of mudrocks interbedded with sandstones and carbonates in a deep- water foreland basin that had poor circulation with the open ocean. The cyclic sedimentation and basin tectonics resulted in a complex stratal architecture that was sourced by multiple areas of sediment input. Previous studies of the Cherokee Group focused on age-equivalent strata in Oklahoma and Kansas. This study uses six cores and 1980 wireline logs to characterize facies and their distribution, interpret depositional environment, and construct regional stratigraphic framework. Wireline logs were correlated in the area of over 9500 sq km to map out five depositional packages that are separated by major flooding events. These events are correlative over the whole area of study. Lithofacies are recognized based on depositional features and mineralogy: (1) mud-clast conglomerate, (2) muddy matrix conglomerate, (3) sandy siliciclastic conglomerate, (4) massive sandstone, (5) planar-laminated to ripple cross-laminated sandstone, (6)

laminated calcareous to siliceous mudstone, (7) very thin to thin- laminated argillaceous mudstone, (8) massive to faintly laminated siliceous mudstone, (9) disorganized and/or disturbed laminated mudstone, (10) grainstone and grain-dominated packstone, and (11) peloidal packstone.

The integration of isopach maps of depositional packages with the lithofacies allowed the delineation of the spatial and temporal evolution of the slope to basin-floor system. The Cherokee benthic biota was transported to the basin from the shelf or oxygenated upper slope by gravity flows. Biogenic planktonic sediment was sourced from water column. Deposition of the sandstones and carbonates are by turbidity currents, slurry flow, debris flow, and mud flow. Fine-grained sediments were transported by turbidity currents or by hemipelagic settling. The deposition of the Cherokee Group in the study area occurred under dysaerobic to anaerobic bottom conditions developed below storm-wave base and below the oxygen-minimum zone as evidenced by rare bioturbation, low fauna diversity, high TOC, and high Mo content in the mudrock facies.

Table of Contents

List of Tables

List of Figures

INTRODUCTION

The Middle Pennsylvanian Cherokee Group of the deeper Anadarko Basin (Figure 1) is composed of a mixture of sandstone, limestone, and mudstone. The Cherokee Group was one of the more active exploration targets in the 1990's, and continues to be an active target for conventional sandstone reservoirs (such as the Red Fork and Skinner sandstones) as well as tight-sandstone reservoirs (granite-wash deposits) in the Anadarko Basin. Much of the past effort has been devoted to understanding the stratigraphy, depositional environments, and characterization of conventional reservoirs in age-equivalent shallower water lithofacies. However, little has been published on slope and basinal strata in the Anadarko Basin in the Texas Panhandle. None of the previous studies evaluated the mudstones in the Cherokee Group as potential unconventional reservoirs. Glass (1981), Whiting (1982), Udayashankar (1985), Schneider and Clement (1986), and Anderson (1992) published general reviews on the Anadarko Basin geology, established the basinal stratigraphic framework, and interpretations of depositional facies. Oakes (1953) divided the Cherokee Group into two sections, known as Krebs (upper) and Cabaniss Groups (lower) in the adjacent Arkoma Basin. The Oklahoma geological survey prepared a series of special publications on the productive formations in the Cherokee Group in Oklahoma, including the informal Skinner and Prue sandstone (Andrews et al., 1996), which are the uppermost unit of the Cherokee Group, and Red Fork sandstone (Andrews and Rottmann, 1997) and the Bartlesville sandstone (Northcutt and Andrews, 1997) from the lower Cherokee Group. The publications include an overview of the regional stratigraphy, sandstone distribution, depositional models, and production case studies. The informal Red Fork sandstone is considered as submarine fan, stacked channel-fill deposits (Al-Shaieb et al., 1994; Puckette et al., 2002), and the Prue-Skinner sandstone was interpreted to be

deposited in fluvial-deltaic shallow-water marine environments (Andrews et al., 1996; Boucher, 2009) in Oklahoma. The Morrowan to Permian granite-wash reservoirs were found in the deeply buried (at least 10,000 ft [3028 m]) Anadarko Basin immediately adjacent to the Wichita-Amarillo Mountain uplift. They are generally considered to be deposited within alluvial fan and fan-delta environments. Some granite-wash sediments bypassed the shelf and were transports into deeper water slope and basinal environments by turbidity and debris flows (Mitchell, 2011).

Figure 2 depicts the stratigraphy of the Middle Pennsylvania System. The lower Desmoinesian Cherokee Group is underlain by the Atoka Group and overlain by the Marmaton Group. The figure lists informal subsurface formation names from previous studies in Oklahoma (Higley, 2014).

Recent production targets of the Pennsylvanian section in the Texas Panhandle are in the Desmoinesian granite-wash deposits, the Marmaton/Cleveland sandstones and Atoka limestones/shales. The extensive production and study on the Cherokee Group in Oklahoma suggests that the Cherokee Group contains both good reservoirs (e.g., the Red Fork sandstone) and source rocks (Burruss and Hatch, 1989; Higley, 2014). The interbedded organic-rich mudstone facies and sandstone facies make the Cherokee Group a potential candidate for being a hybrid mudstone system. Because of the understudied area of the Cherokee Group in the Texas Panhandle, the investigation of the stratigraphic architecture, lithofacies, and depositional setting was undertaken, using wireline logs and cores from Ochiltree, Robert, Hemphill, and Lipscomb Counties, Texas Panhandle (Figure 1). The major objectives of this investigation are to (1) document the detailed stratigraphic architecture, lithofacies types of the Cherokee Group in the Texas Panhandle, and understand the relationship between the deposits and associated depositional processes, especially of the fine-grained sedimentary rocks, (2) characterizes depositional

environments and lithofacies distribution, (3) assess reservoir quality of the sandstones and mudstones of this hybrid system and discuss hydrocarbon potentials for conventional and unconventional reservoirs in study area, and (4) generate a depositional model as an analog for similar systems. The results of this investigation can be used to enhance the understanding of the area of investigation for future exploration and can provide an analog for understanding lithofacies distributions in similar subsurface analogous sandstone/mudstone hybrid systems.

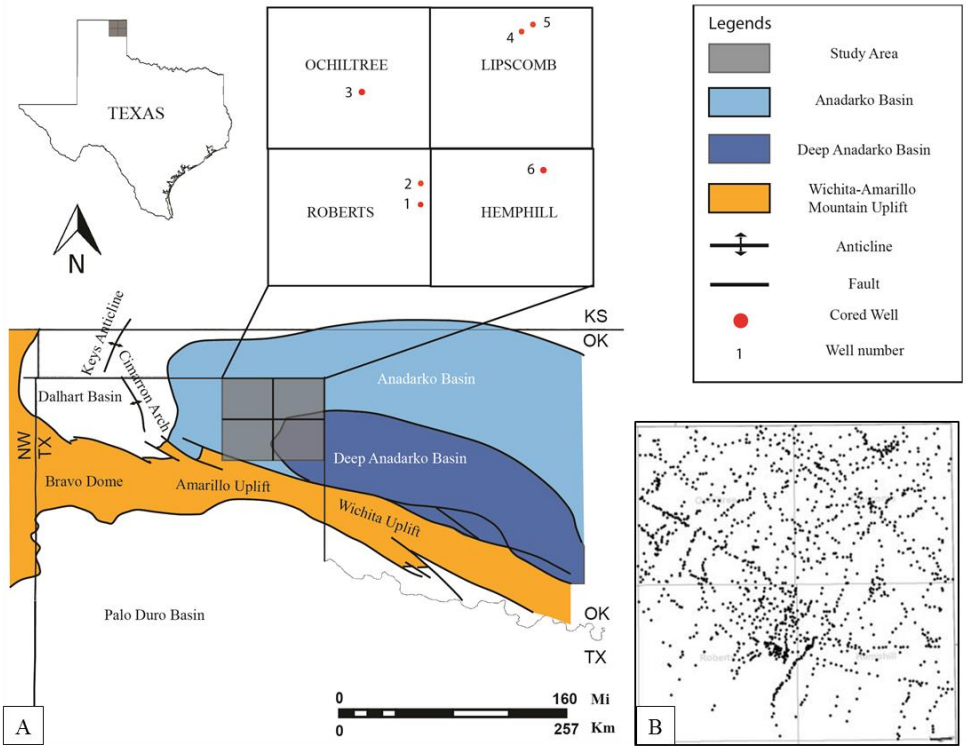

Figure 1. (A) Map of the northwestern part of the Anadarko basin showing the study area, general structural features, and location of cores (Flowers Trusts No. 3-8 [1], Marjorie Campbell No. 1 [2], Sam Hill No. 2-A [3], Kuhlman No. 3-A [4], Schoenhal No. 1 [5], and Rio Bravo No. 2 [6]). Map modified from Ambrose (2011). (B) Location of the wells that were used in the stratigraphic correlation.

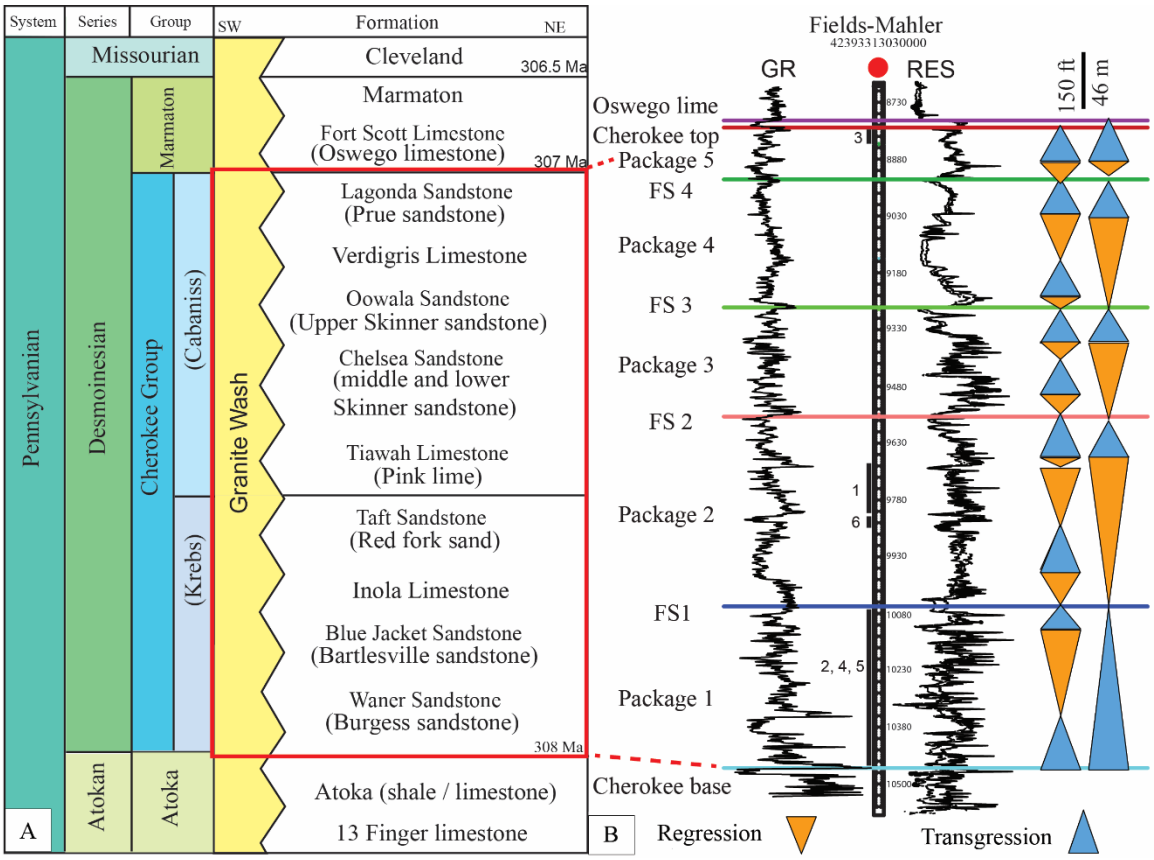

Figure 2. (A) General stratigraphy of the Cherokee Group in the northwestern Anadarko Basin in Texas Panhandle, showing the formal surface names and the commonly accepted subsurface names (in parenthesis) used in Oklahoma. Figure is modified from Ambrose (2011), Higley (2014), and Mitchell (2014). (B) Type wireline-log of the Cherokee Group with flooding surfaces, depositional packages, and depositional cycles. See well names in Figure 1.

DATASET AND METHOD

Data and interpretations presented in this paper were derived from the investigation of six cores (Figure 1A) totaling 634 feet (193 m) and correlation of 1980 wireline-logs that were gridded evenly throughout the study area (Figure 1B). Cores were described for sedimentary features, fabric and texture, and minerology for interpretation of lithofacies and sedimentary processes.

One hundred and thirty-nine polished thin sections were prepared and analyzed under an optical microscope for rock fabric, texture, biotic content, mineralogy, and pore network. Thin sections were stained with sodium-cobalt nitrite for potassium feldspar identification and alizarin red and potassium ferrocyanide for carbonate identification.

Eighty-four samples were analyzed by K-T GeoServices, Inc. for mineralogy by x-ray diffraction (XRD) analysis (Figure 3). Routine core analyses (permeability, porosity, and grain density) were obtained for forty-seven coarse-grained samples by Weatherford Laboratories (Figure 4). Leco TOC, Rock-Eval analyses, and maturity analyses (Figure 5) were performed by GeoMark Research, Ltd on thirty-nine fine-grained samples to determine organic geochemical properties.

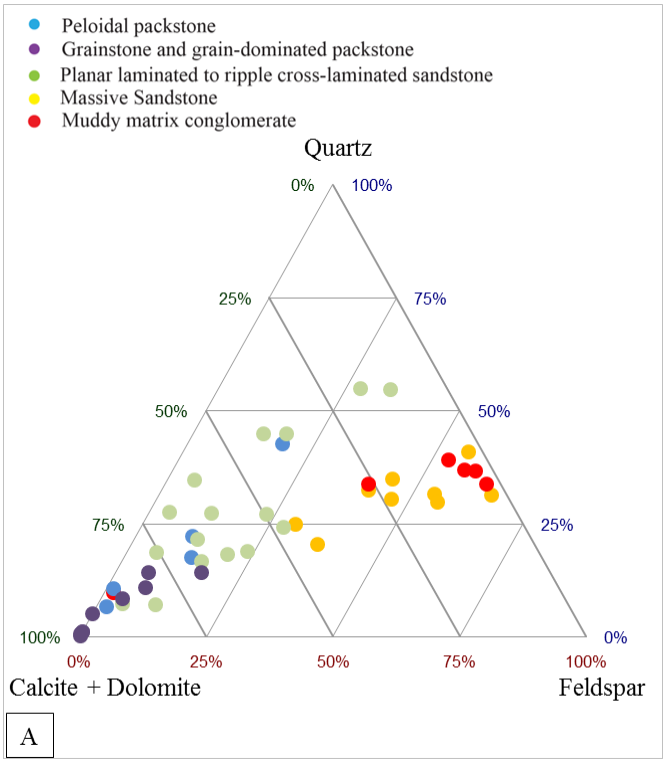
Peloidal packstone
Grainstone and grain-dominated packstone
Planar laminated to ripple cross-laminated sandstone
Massive Sandstone
Muddy matrix conglomerate
Quartz
0%
100%
25%
75%
50%
50%
75%
25%
100%
0%
0%
25%
50%
75%
100%
Calcite + Dolomite
Feldspar
A

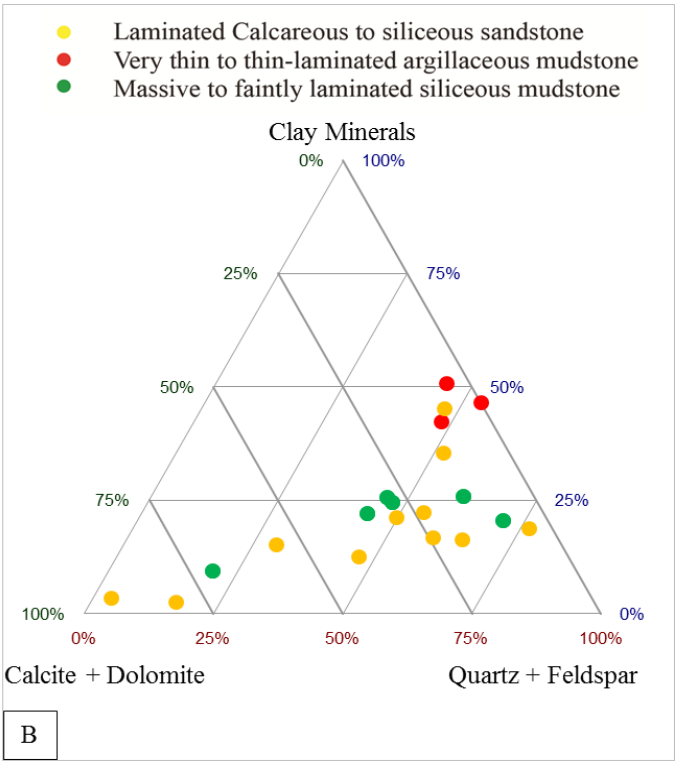
Laminated Calcareous to siliceous sandstone
Very thin to thin-laminated argillaceous mudstone
Massive to faintly laminated siliceous mudstone
Clay Minerals
0%
100%
25%
75%
50%
50%
75%
25%
100%
0%
0%
25%
50%
75%
100%
Calcite + Dolomite
Quartz + Feldspar
B

Figure 3

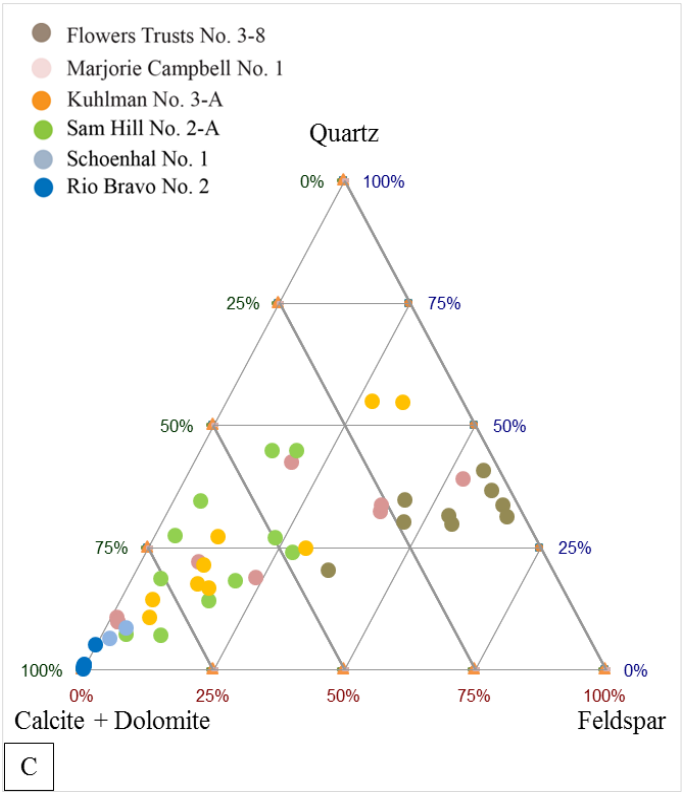

Figure 3. Ternary diagrams of Cherokee Group mineralogy. Data is based only on X-ray-diffraction derived average composition. (A) Conglomerate, sandstone and carbonate mineralogy by lithofacies. (B) Mudstone mineralogy by lithofacies. (C) Conglomerate, sandstone and carbonate mineralogy by wells. Well locations see Figure 1.

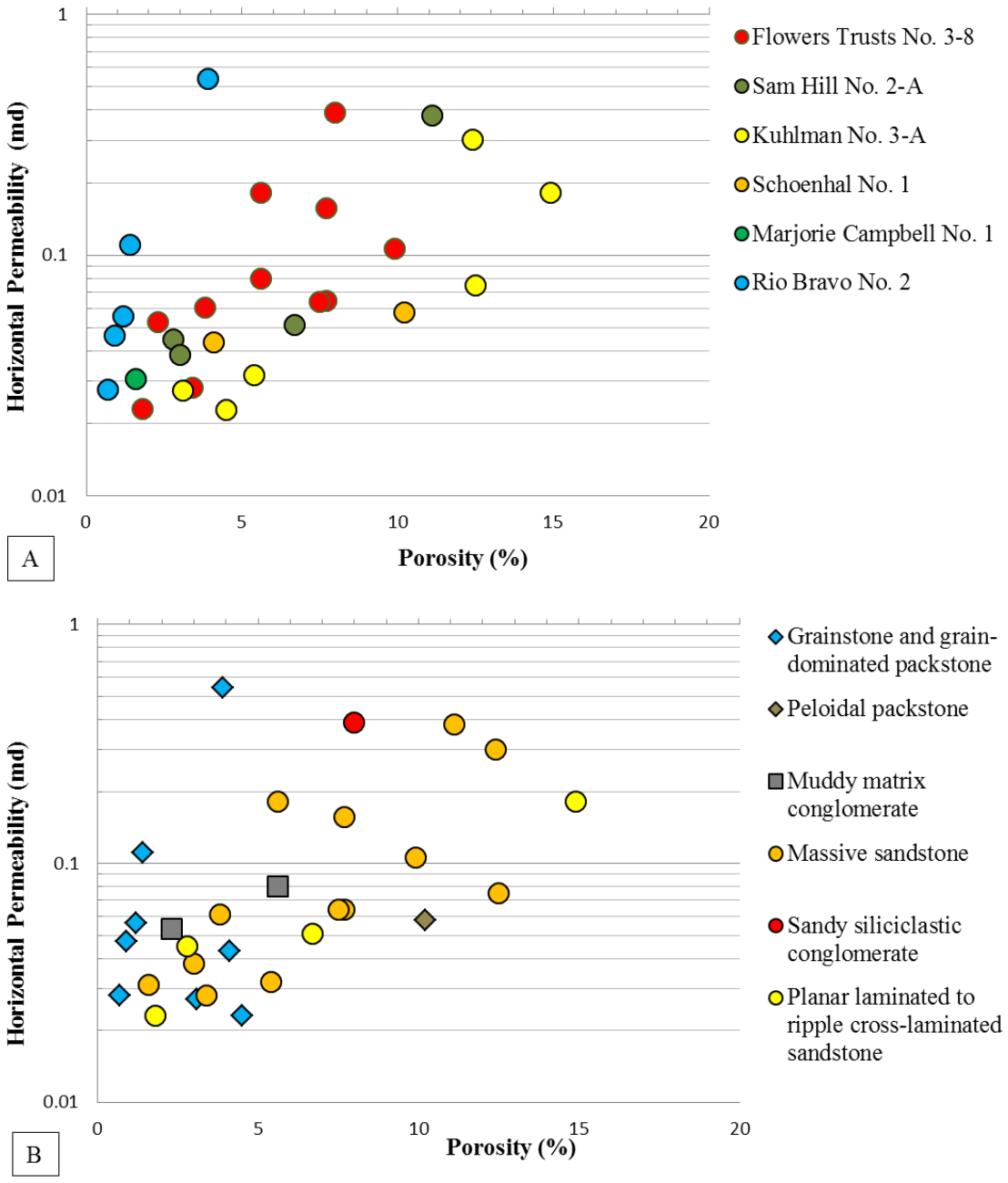

Figure 4. Porosity versus permeability for samples in the study area. (A) Porosity-permeability relationship by wells. (B) Porosity-permeability relationship by lithofacies.

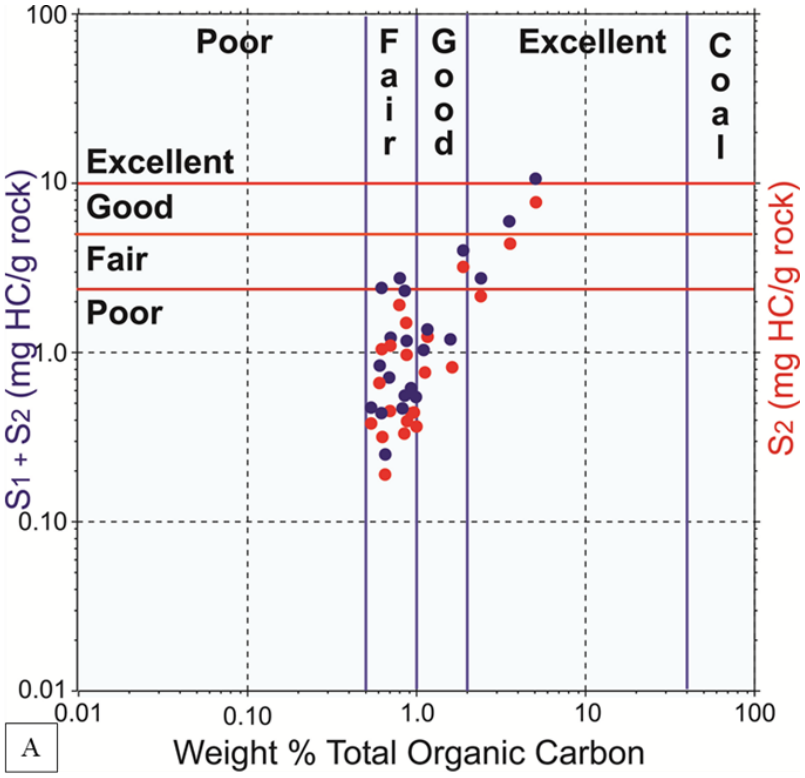

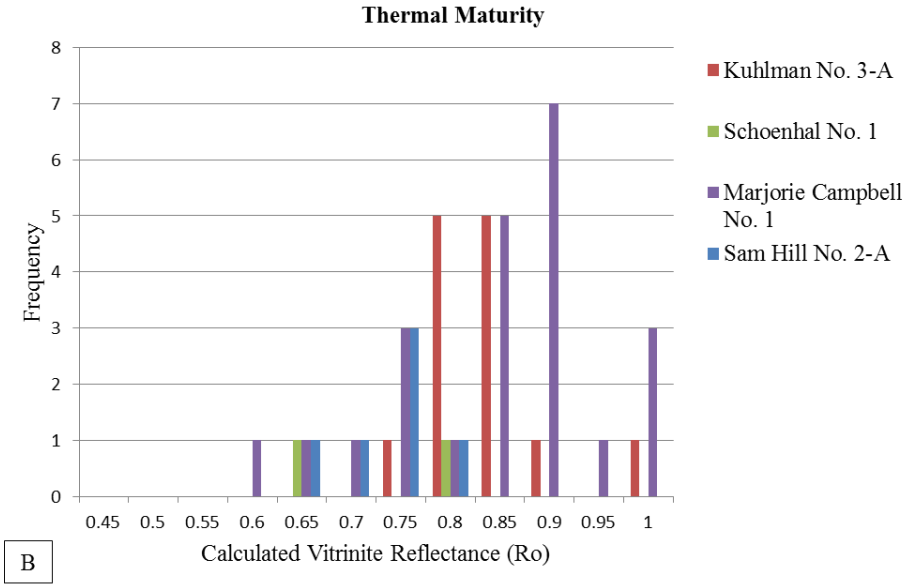

Figure 5. (A) Classification of Kerogen Quantity using Dembicki's (2009) Scheme based on RockEval data. S1 values are generated hydrocarbons, S2 values are hydrocarbon-generating potential. B) Histogram of calculated vitrinite reflectance showing source rock maturity. Mean Ro is 0.84%. All samples are in oil window (0.6-1.1 %) (Dow, 1977).

High-resolution energy dispersive x-ray fluorescence data were collected by ED-HHXRF (Energy Dispersive Hand-Held X-Ray Fluorescence) at 2 inch intervals on Marjorie Campbell No. 1 core. Major elemental data acquisition, which included V and Cr measurements, was undertaken on a low-energy, vacuum-pumped instrument setting for a 60-second count time; trace elemental data acquisition was undertaken on a high-energy, Al-filtered instrument setting for a 90-second count time. Both major and trace elements data were collected at the same location on the cleaned core face. The XRF calibration method was derived by Rowe et al. (2012) on the basis of samples from various mudrock formations.

Regional stratigraphic framework was constructed by correlating 1980 wireline logs in an area of over 9500 sq km (Figure 1) on a Petra project. Five depositional packages were defined and each package is separated by a major flooding surface. Stratigraphic tops were picked from gamma-ray and resistivity curves. The type wireline log is presented in Figure 2 and shows the stratigraphic tops used in the investigation. Average well density throughout most of the study area is approximately 0.2 well/mi^2; some sections of the study area have greater well density, which allows increased accuracy in mapping of unit thicknesses, structures, and gross-sandstone trends. Wireline-log data were utilized to support sedimentologic and stratigraphic interpretations where core coverage was lacking. The core-to-log depth was calibrated by correlating the GR signature with the core description. Clay-mineral-rich and TOC-rich intervals were matched to high GR readings. Lithofacies and cycle patterns from core description were matched with wireline-log responses. Gross sandstone was counted from slabbed core and calibrated to gamma ray log response. The inflection point of sandstone and mudstone was used for determine gross sandstone. Gross-sandstone thickness was calculated for each package and then isopachous maps were generated according to the calculated data.

GEOLOGICAL BACKGROUND

The Anadarko Basin is an asymmetric, northwest-southeast-trending basin with its axis lying close to the southern margin (Rascoe and Johnson, 1988). The study area (Ochiltree, Robert, Hemphill, and Lipscomb Counties in Texas Panhandle; Figure 1) is located in the northwestern part of the Anadarko Basin, which is bounded to the south by the Wichita-Amarillo Mountain uplift, to the northwest by the Cimarron Arch (Rascoe and Adler, 1983; Johnson et al., 1988), and to the north by the Kansas Shelf (also known as the Northern Shelf) (Hentz, 2011). Further east, the Anadarko Basin is bounded by the Nemaha Ridge (Rascoe and Johnson, 1988). Maximum structural displacement between the Wichita Mountain uplift and the basin floor exceeds 30,000 ft (9144 m) (Al-Shaieb and others, 1994). Evans (1979) suggests that maximum subsidence of the basin occurred during Morrowan and Atokan times. Strike-slip faulting was relatively minor and late, with most occurring during the Permian (Higley, 2014).

The Cherokee Group was deposited during Desmoinesian time when the Anadarko Basin was actively subsiding (Whiting, 1982). Dominant source areas for the Pennsylvanian basin fill are the Kansas Shelf to the north and the Wichita-Amarillo Mountain uplift to the south (Figure 1) (Hentz, 2011; Higley, 2014). Local Cherokee paleogeography, which is based on formation-thickness trends, was also influence by the northwest-trending Lips Fault (Figure 6) in Hemphill, Roberts, and Ochiltree Counties (Evans, 1979; Ambrose, 2011).

Global plate reconstructions by Blakey (2013) suggest that during Desmoinesian time, the Anadarko Basin area occupied a narrow inland seaway between Laurussia and Gondwana (Figure 7). Estimated mean water depth on shelf is 249-315 ft (76-96 m) (Moore, 1958, 1964; Heckel, 1977; Gerhard, 1991; Algeo and Heckel, 2008) and up to 492

ft (150 m) during sea-level highstand (Heckel, 1977). Water depth in the deep basin was estimated as several hundred meters and varied through time in response to episodes of basin subsidence and fill (Algeo and Heckel, 2008). The shelf was distinguished from the basin by a hinge line that marks the abrupt increase in rate of thickening form the shelf (10 ft/mile [1.9 m/km]) into basin (50 ft/mile [9.5 m/km]) (Rascoe, 1962). Study area is located in the deep basin according to the paleogeography map (Rascoe and Adler, 1983). Given the magnitude of the relative sea-level drop (up to 150 ft [45 m]) postulated by Ross and Ross (1987) and estimated hundreds of meters' water depth (Algeo and Heckel, 2008), the study area was probably deep enough to not have been affected by storm waves during sea-level lowstands. Algeo and Heckel (2008) suggested that the oxygen-minimum zone rose to less than 100 m (328 ft) water depth in the Mid-continent Sea during Pennsylvanian time. Anoxic bottom water condition was established by the pycnocline that inhibited long-term vertical circulation of oxygenated surface waters to the bottom and allow the preservation of a large amount of organic matter (Heckel, 1991; Algeo and Heckel, 2008).

The Cherokee Group strata of the western Anadarko Basin are underlain by early Pennsylvanian carbonates (Atoka group carbonates), and overlain by middle Pennsylvanian sandstones and carbonates (Marmaton group sandstone and carbonates, e.g., Oswego Limestone) (Figure 2). The Cherokee group in the study area is thickest along the Wichita-Amarillo Mountain uplift and thinning toward northwest (Figures 8, 9). The paleogeography map published by (Rascoe and Adler, 1983) demonstrates that the deepest part of the Anadarko Basin (on the basis of sediment thickness) was to the southeast in Oklahoma.

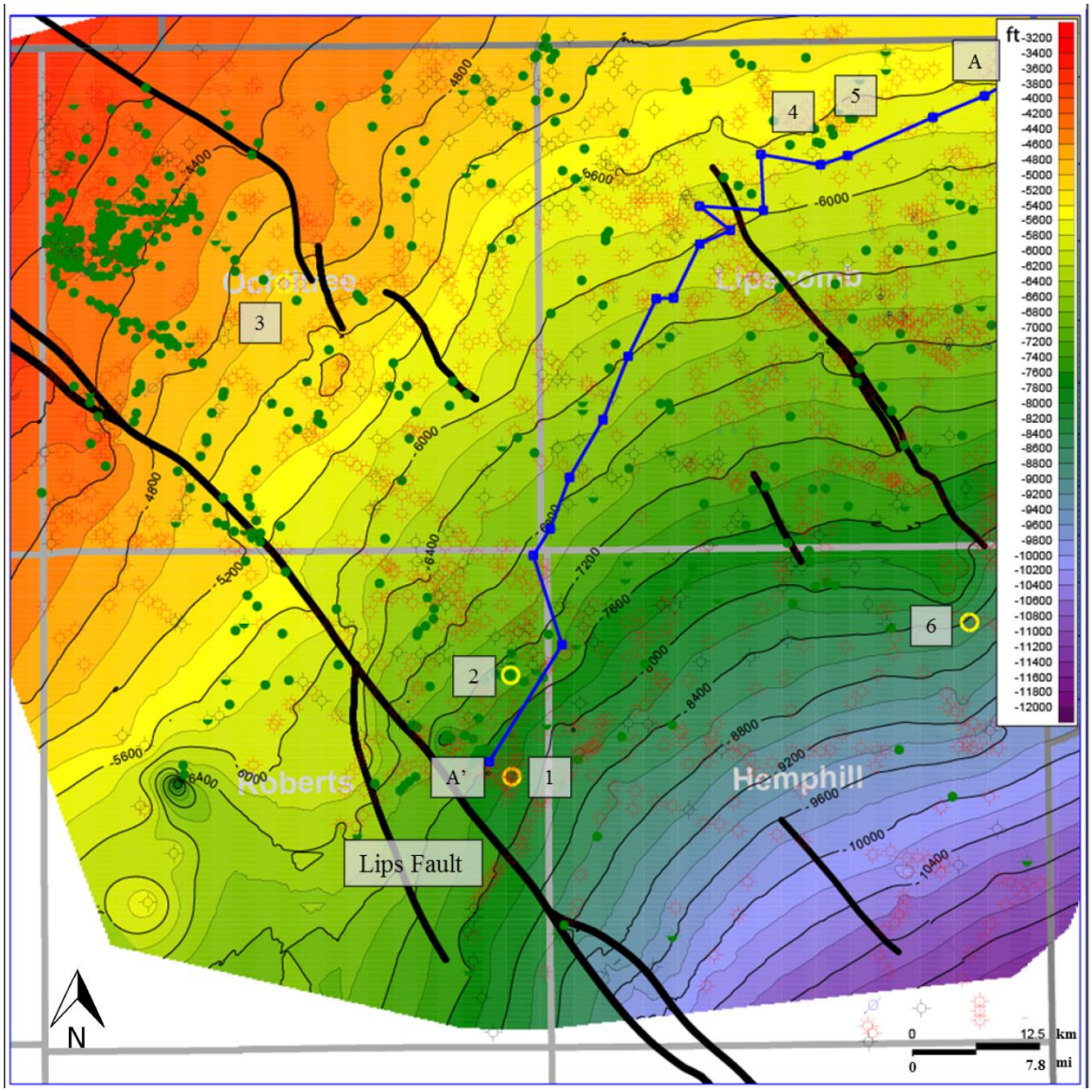

Figure 6. Structure contour map of the base of the Cherokee Group. Cored wells are marked as yellow. Cross section is shown in Figure 9. See well names in Figure 1.

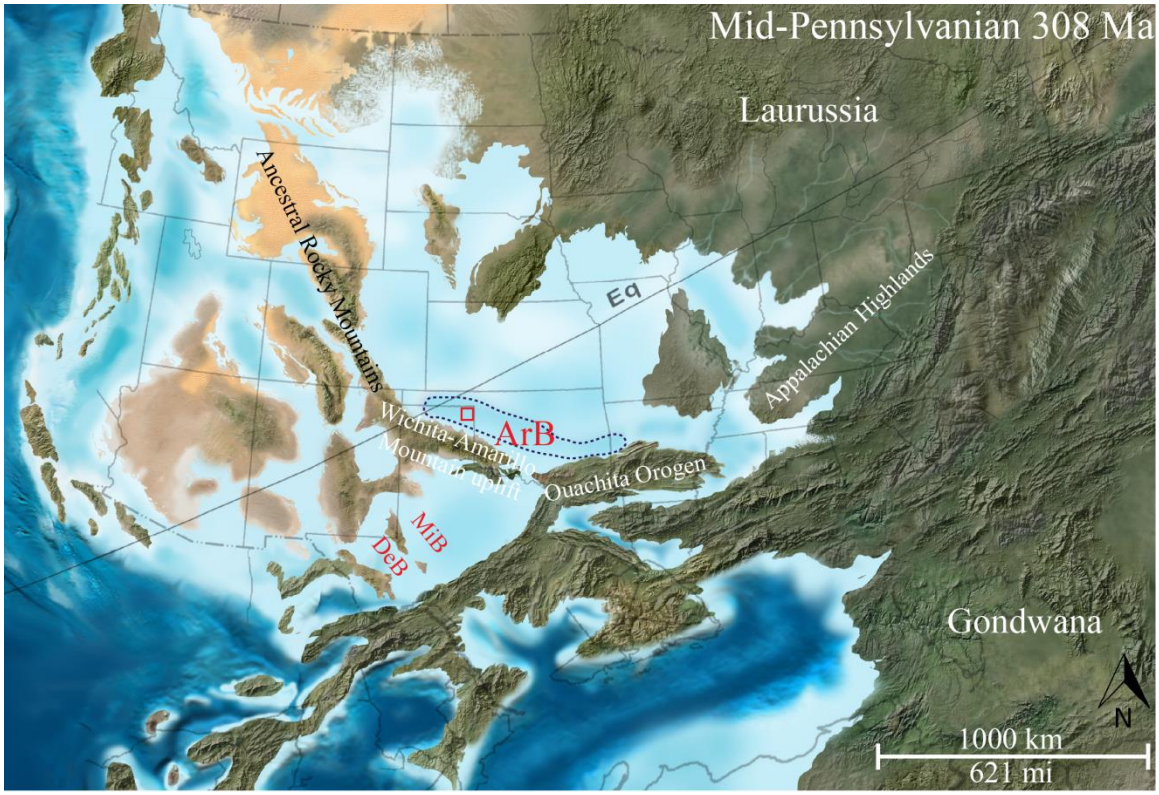

Figure 7. Regional paleogeography of the southern midcontinent region during the middle Pennsylvanian (308 Ma) showing the approximate location of the Anadarko Basin (ArB), Midland Basin (MiB) and Delaware Basin (DeB). Plate reconstruction by Blakey (2005).

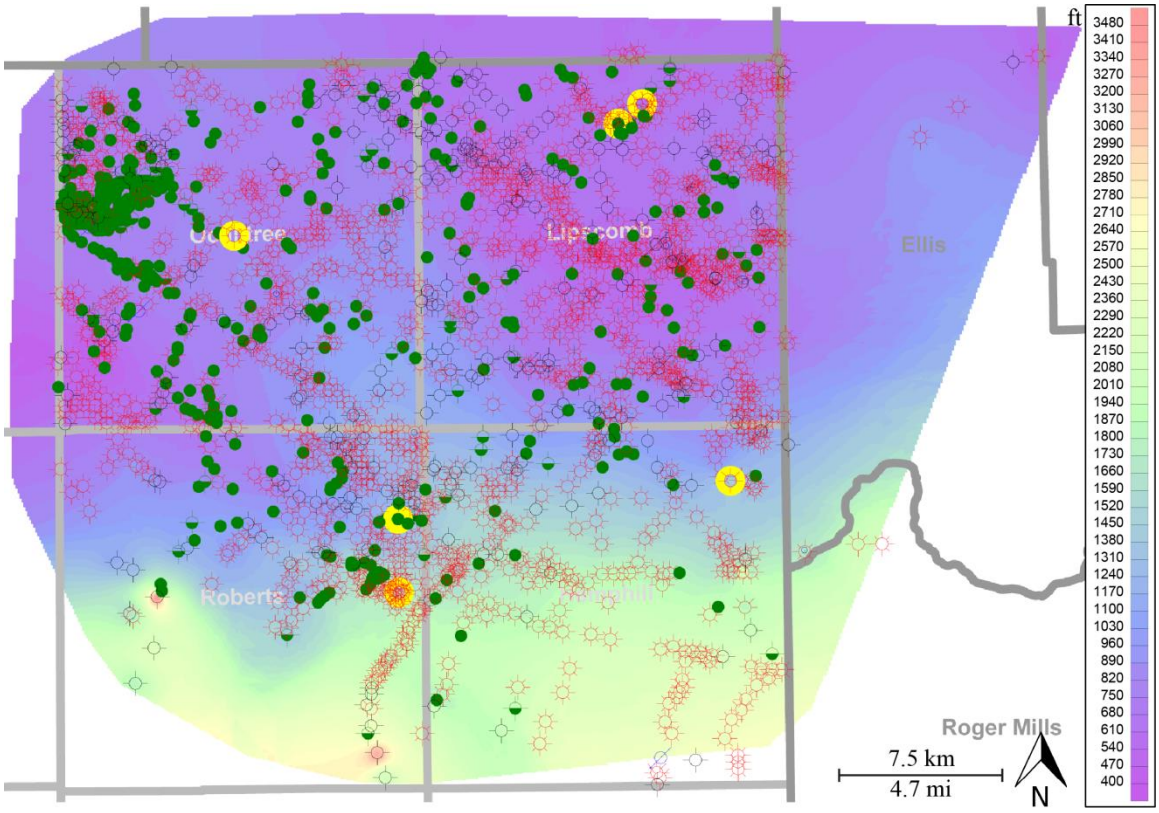

Figure 8. Isopach map of the Cherokee Group, Texas Panhandle.

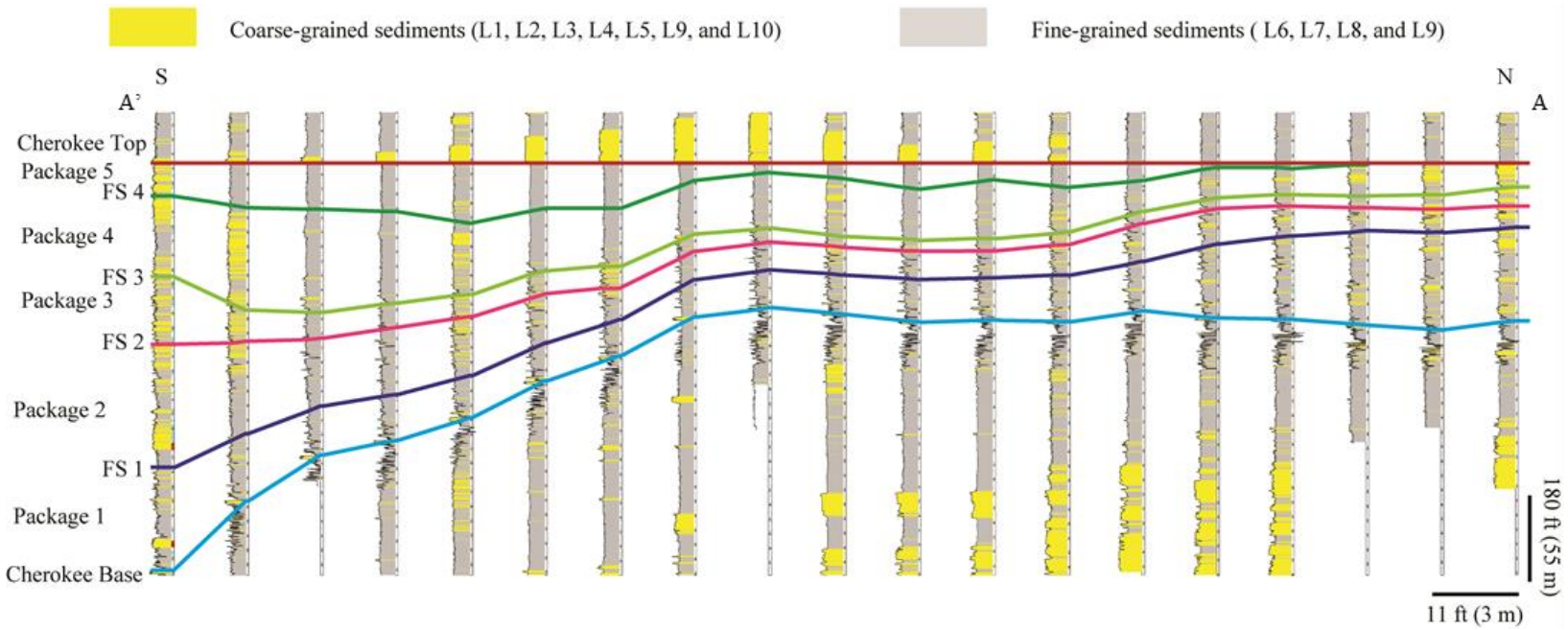

Figure 9. Regional cross section of the Cherokee Group constructed from well data. Section is flatten on the top of Cherokee Group (low-gamma-ray interval). Cross section wells are marked on figure 6.

LITHOFACIES

The Cherokee interval is composed of a variety of lithofacies, which can be divided into coarse-grained lithofacies with differing reservoir quality and fine-grained lithofacies that show a range of hydrocarbon generation potentials. Eleven general lithofacies are defined on the basis of mineralogy, fabric, texture, and biota (Table 1): (1) mud-clast conglomerate, (2) muddy matrix conglomerate, (3) sandy siliciclastic conglomerate, (4) massive sandstone, (5) planar-laminated to ripple cross-laminated sandstone, (6) laminated calcareous to siliceous mudstone, (7) very thin to thin- laminated argillaceous mudstone, (8) massive to faintly laminated siliceous mudstone, (9) disorganized and/or disturbed laminated mudstone, (10) grainstone and grain-dominated packstone, and (11) peloidal packstone.

Cherokee lithofacies were defined from the analysis of six cores. The most complete cored section is from the Marjorie Campbell No. 1 well (Figure 1) in Roberts County. This core recovered 279 ft (85 m) of section, which is almost the entire intervals for Package 1 (Figure 2, discussed below). The other core from Robert County, the Flowers Trusts No. 3-8 (86 ft [26 m]) includes the arkosic conglomerate lithofacies (granite-wash deposits) and represents a part of Package 2 (Figures 1, 2, discussed below). The cores from Kuhlman No. 3-A (112 ft [34 m]) and Schoenhal No. 1(36 ft [11 m]) well located at the Lipscomb County (Figure 1) recovered partial intervals of Package 1. The Sam Hill No. 2-A core (80 ft [24 m]; discontinuous) is located in Ochiltree County (Figure 1) and contains the uppermost interval of Package 5 (Figure 2, discussed below). The core from Rio Bravo No. 2 well (33 ft [10 m]; discontinuous) located in Hemphill County recovered a short interval of Package 3 (Figures 1, 2, discussed below).

Elemental data collected by handhold XRF on Marjorie Campbell is used to distinguish mudstone facies and aid in interpreting conditions of the depositional environment. Elemental proxy categories are (Calvert and Pedersen, 2007): 1) siliceous indicators: Si, 2) terrigenous input: Ti, K, Zr, Th, Ga, Cr, Al, 3) calcareous indicators: Ca, Sr, Mn, Mg, 4) oxygen-level: Mo (anoxia), and Zn, V, Cu, Ni (suboxic).

Table 1. Lithofacies of the Cherokee Group

Lithofacies	Name	Sedimentary texture	Sedimentary massive	Bounding surfaces	Lithologic accessories	Bioturbation	Depositional process	Appearance
L1	Mud-clast conglomerate	Fine- to medium-sand size, medium sorted, sandy to muddy matrix. Coarse-sand to pebble size, poorly sorted mud intraclast.	Aligned mud-clasts	Sharp base and top	Pebble-size mud-clasts	Rare	High-density turbidity current and erosive	MC and FT
L2	Muddy matrix conglomerate	Coarse-sand to granule-size conglomerate, siliciclastic and carbonate clasts	Generally massive	Sharpe base, gradual top		Rare	Siliciclastic debris flow and calcareous mud flow	MC and FT

Table 1 (continued)

L3	Sandy siliciclastic conglomerate	coarse-sand to pebble-size grain, very-fine sand to medium arkosic sand matrix	Graded, massive	Sharp base, sharp to gradual top	Mud-clasts	Rare	High-density turbidity current	MC and FT
L4	Massive sandstone	Poorly sorted, fine- to very coarse sand size	Generally massive, dish structure, and inversely graded layers (locally)	Sharp base, sharp top	Rip-up clasts	Rare	High-density turbidity current	FT, MC

Table 1 (continued)

L5	Planar laminated to ripple cross-laminated sandstone	Very fine to coarse-sand size	Traction structures, trough-stratifications, and climbing ripple	Sharp base, sharp to gradual top	Organic detritus	Rare	High-density turbidity current and low-density turbidity current	SH, K, S, FT, MC
L6	Laminated calcareous to siliceous mudstone	Grains are silt size and are calcareous to siliceous	Planar to cross laminated	Gradual to sharp base	Skeletal grains, fine-grain peloids, organic flakes	Rare to abundant (laminae are destroyed)	Low-density turbidity current	K, S, FT, MC, SH

Table 1 (continued)

L7	Very thin to thin-laminated argillaceous mudstone	Clay-size minerals dominant	Wavy, very thin to thin laminations	Gradual to sharp base	Organic flakes	Rare	Turbidity currents and reworking by bottom currents	K, MC
L8	Massive to faintly laminated siliceous mudstone	Silt to clay size	Nonlaminated to faintly laminated	Gradual to sharp base	Skeletal grains, fine-grain peloids, organic flakes	Rare	Hemipelagic settling	K, MC, FT

Table 1 (continued)

L9	Disorganized and/or disturbed laminated mudstone	Silt to clay size	Soft-sediment deformation, microfaulting	Sharp to gradual top and base		Rare	Slumping/sliding	MC, FT
L10	Grainstone and grain-dominated packstone	Coated grains and skeletal grains	Laminated	Sharp to gradual top and base		Rare	Turbidity currents	K, S, SH, RB
L11	Peloidal packstone	Silt- to fine-sand size peloids	Massive	Sharp to gradual top and base		Rare	Turbidity currents	MC, K, S
	MC	Marjorie Campbell No. 1	S	Schoenhal No. 1	RB	Rio Bravo No. 2		
	FT	Flowers Trusts No. 3-8	SH	Sam Hill No. 2-A	K	Kuhlman No. 3-A		

Lithofacies 1 (L1): Mud-clast conglomerate

The mud-clast conglomerate lithofacies is composed of coarse-sand to pebble-size mud-clasts supported by sand-matrix (Figure 10A) and sandy mud-matrix (Figure 10B). The former is more common with the mud-clasts floating in a matrix of well to moderately sorted sandstone. Lower contacts are commonly sharp, while upper contacts range from sharp to gradational. The mud-clasts are subrounded to angular, generally elongate, imbricated to weakly imbricated, and composed of soft, dark gray mudstone.

Lithofacies 2 (L2): Muddy matrix conglomerate

The muddy matrix conglomerate lithofacies consists of coarse-sand to granule-size grains supported by very fine silt- to clay-size muddy matrix. Grains are predominately siliciclastic (Figure 10D, E), however, gravel-size calcareous grains were overserved in one interval (Figure 10F, G). L2 appears to have no internal stratification. Medium- to very coarse sand size mud-clasts are present in some samples.

The muddy matrix conglomerate lithofacies contains an average of 5.2 wt% clay minerals (range: 1.2 to 7.5 wt%). The clay-mineral content is much higher than other sandstone facies (e.g., sandy siliciclastic conglomerate and massive sandstone; Table 2) and grainstone and grain-dominated packstone (Table 2), and is almost as high as in the laminated mudstone lithofacies (mean: 5.9 wt%; Table 2, Appendix 1). However, this lithofacies has much more quartz and feldspar (mean: 23.2 wt%) than the laminated mudstone lithofacies (mean: 14.6 wt%).

Lithofacies 3 (L3): Sandy siliciclastic conglomerate

The sandy siliciclastic conglomerate lithofacies (Figure 10H, I) is composed of coarse-sand to pebble-size grains with a matrix of very fine to medium-grain arkosic sandstone. Quartz (monocrystalline quartz, polycrystalline quartz, and microcrystalline

quartz) and plagioclase are the dominant minerals. Plagioclase is commonly altered to sericite. K-feldspar (orthoclase with perthitic structures and microcline), lithic fragments (granitic and metamorphic), and mud-clast-rock fragments are common. Glauconite, muscovite, biotite, zircon, garnet, and tourmaline are present. Reworked skeletal fragments and peloids are present locally.

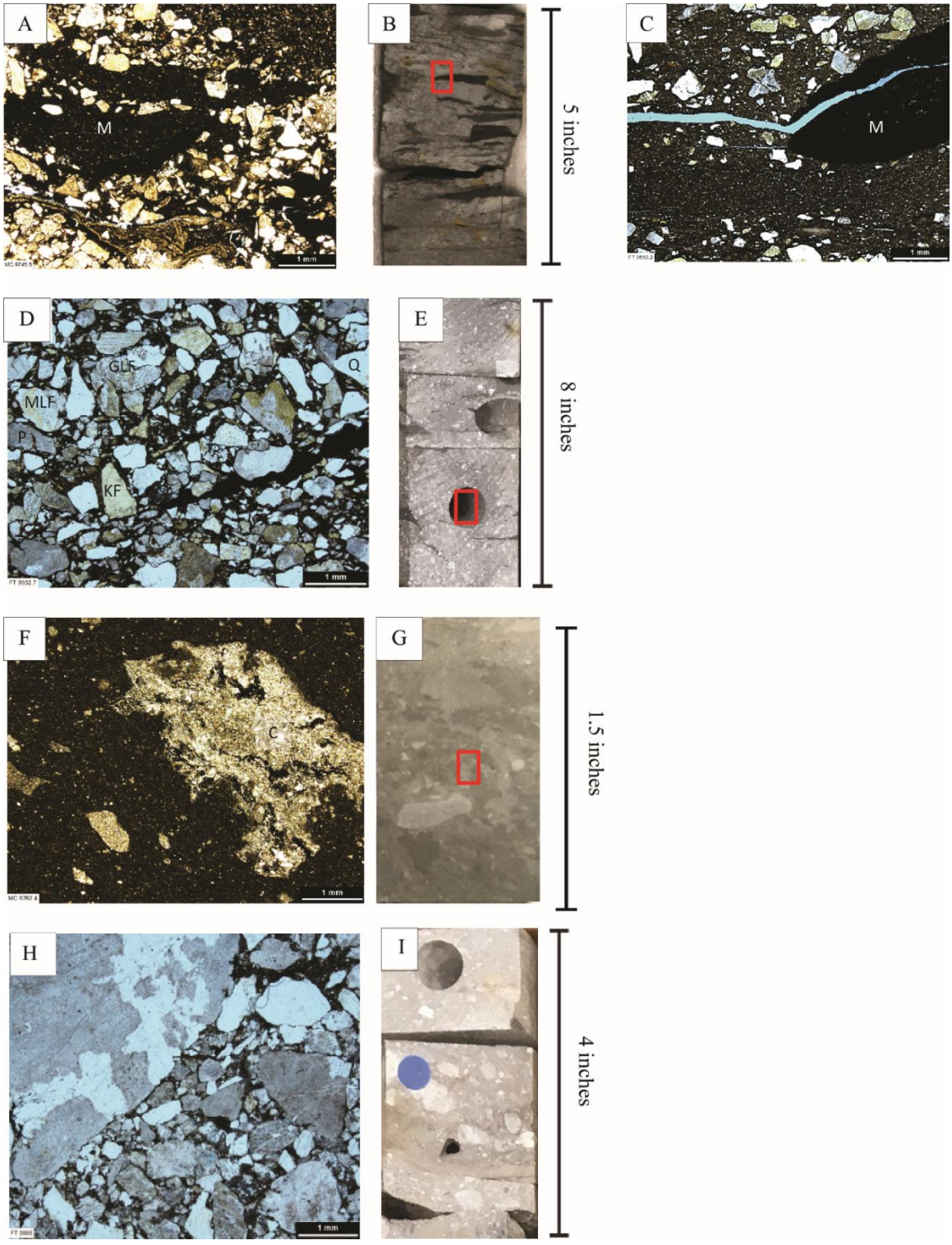
A
M
1 mm
B
5 inches
C
M
1 mm
D
GLF
Q
MLF
P
KF
1 mm
E
8 inches
F
C
1 mm
G
1.5 inches
H
1 mm
I
4 inches

Figure 10

Figure 10. Photographs of conglomerate lithofacies (L1, L2, and L3). M is (A) Photomicrograph of mud-clast conglomerate lithofacies (L1) with sand matrix showing mud-clast (M): Marjorie Campbell No. 1, 9762.4 ft (2976 m). (B) Core photo of L1. Rectangle shows the sample location of the thin section in Figure 10A. (C) Mud-clast conglomerates lithofacies with mud matrix (L1): Flowers Trusts No. 3-8, 9932.7 ft (3027 m). Porosity is 4.9% and permeability is less than 0.001md. (D) Photomicrograph of muddy matrix conglomerates lithofacies (L2) with siliciclastic grains including K-feldspar (KF), quartz (Q), granitic lithic fragment (GLF), plagioclase (P), and metamorphic lithic fragment (MLF): Flowers Trusts No. 3-8, 9932.7 ft (3027 m). Porosity is 2.3% and permeability is 0.053 md. (E) Core photo of L2. Rectangle shows the sample location of the thin section in Figure 10D. (F) Photomicrograph of muddy matrix conglomerates lithofacies (L2) with calcareous grains (C): Marjorie Campbell No. 1, 7762.4 ft (2366 m). Porosity is 4.9% and permeability is less than 0.001md. (G) Core photo of L2. Rectangle shows the sample location of the thin section in Figure 10F. (H) Photomicrograph of sandy siliciclastic conglomerate lithofacies (L4): Flower Thrust No. 3-8, 9865 ft (3006 m). (I) Core photo of L3. Rectangle shows the sample location of the thin section in Figure 10H.

Lithofacies 4 (L4): Massive sandstone

Massive sandstone lithofacies (Figure11A, B) is moderately to poorly sorted, fine- to very coarse sand size. Mud-clasts occur within beds, especially at the base. Scours are common at sharp bases. The upper surfaces are commonly sharp. Amalgamation of beds is observed and the contact surfaces are defined by aligned mud-clasts or grain-size breaks.

Quartz (monocrystalline quartz, polycrystalline quartz, and microcrystalline quartz; mean: 10.4 wt%, range: 6.5 to 14 wt%) and plagioclase (mean: 12.5 wt%, range: 8.5 to 14.7%) are the dominate minerals. Plagioclase is commonly altered to sericite. Other common minerals are K-spars (orthoclase with perthitic structures and microcline, mean: 4.0 wt%, range: 0.2 to 6.0 wt%), muscovite, biotite, pyrite, and zircon (Table 2, Appendix 1). Pyrite is presence in the form of euhedral crystals. Pore network consists of interparticle and intraparticle pores. Intraparticle pores are generally secondary resulting from the dissolution of feldspars. Calcite cement is common (mean: 1.7 wt%), and dolomite occurs in some samples (mean: 4.4 wt%). Matrix is siliceous fine-grained sand and clay minerals. Water-escape features such as dish structures are observed. Thin, inversely graded layers are locally overlying the lower contact of this lithofacies.

Lithofacies 5 (L5): Planar laminated to ripple cross-laminated sandstone

The laminated sandstone lithofacies is characterized by traction structures, such as planar lamination (Figure 11C, D) and ripple cross-lamination (Figure11E, G) with gradational to sharp bases. Climbing ripples (Figure 11C) and trough-stratification are observed. Coarse- to very coarse grain sandstone is present as lag deposits.

XRD data (Table 2, Appendix 1) shows that the laminated sandstone lithofacies is composed in averaged of 2.4 wt% clay minerals, 20.2 wt% quartz and feldspar, and 14.7 wt% carbonate minerals. The mineral composition of this facies is similar with the massive

arkosic sandstone lithofacies, but the laminated sandstone lithofacies contains less feldspars (mean: 7.0 wt%) and more carbonate (mean: 20.26 wt%) compared to the massive sandstone lithofacies (mean feldspar: 16.0 wt%, mean carbonate: 6.1 wt%). One possible reason for this difference is that more samples for the massive sandstone lithofacies were taken from wells located in the southern part of study area (Marjorie Campbell No. 1 and Flowers Trusts No. 3-8), while most of the samples for the laminated sandstone lithofacies were taken from wells located in the northern part of study area (Kuhlman No. 1 core; discussed in more detail below). Glauconite and phosphate are present. The grain size of this facies is generally finer (very fine to coarse-sand size) than the massive arkosic sandstone (fine- to very coarse sand size). The grains are subrounded to subangular, and poorly to well-sorted. Interparticle and intraparticle pores are present. Interparticle pores are more common in this lithofacies than in the massive sandstone lithofacies (Figure 11F, G). The laminated sandstone lithofacies is commonly associated with the massive arkosic sandstone lithofacies and laminated mudstone lithofacies.

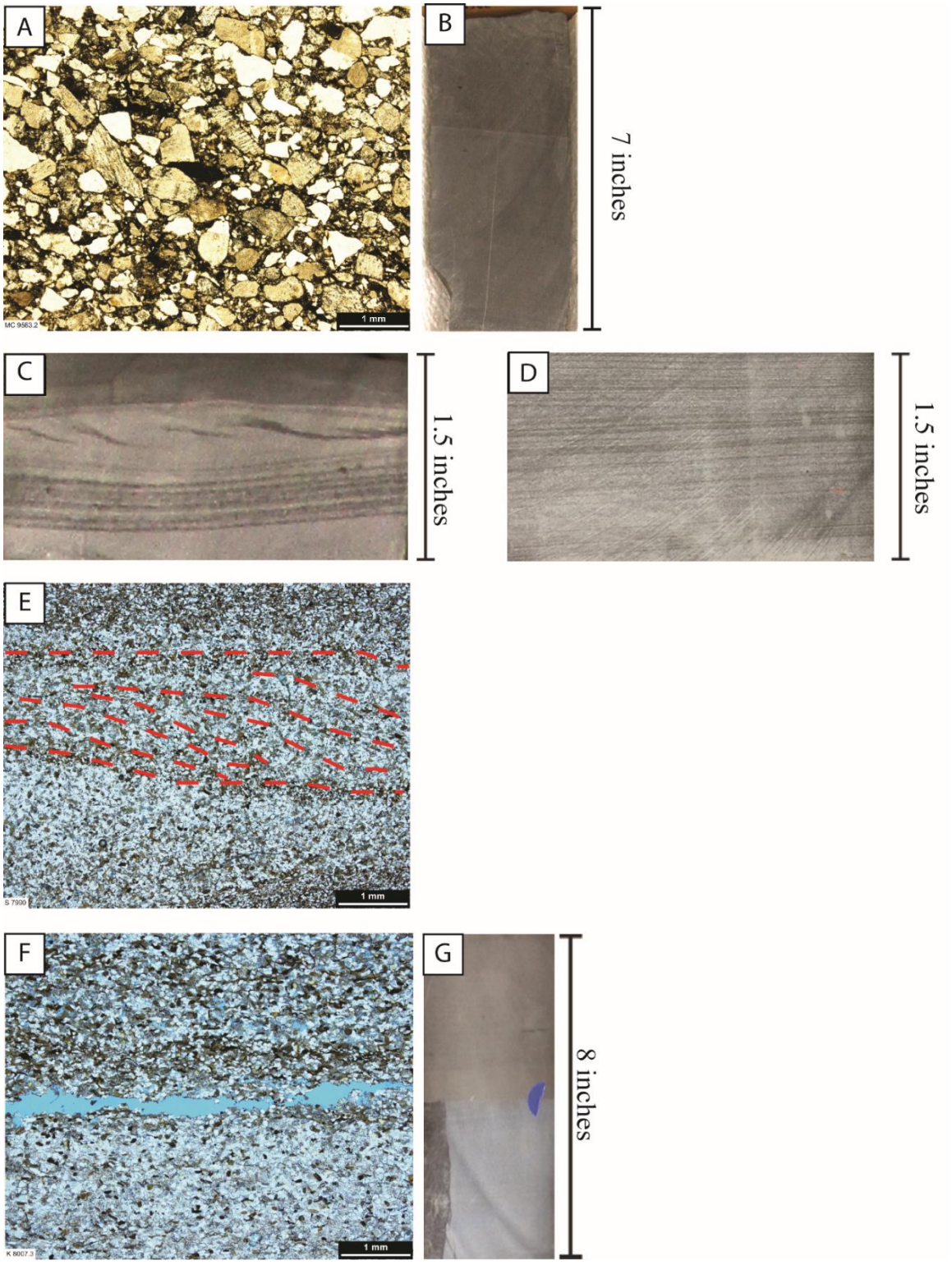

Figure 11

Figure 11. Photographs of sandstone lithofacies (L4 and L5). (A) Massive sandstone conglomerate lithofacies (L4) showing angular to subrounded shape and coarse-sand size grains. Muddy matrix between rigid grains are probably compacted mud-clasts or peloids: Marjorie Campbell No. 1, 9563.2 ft (2915 m). Porosity is 1.6% and permeability is 0.031 md. (B) Core photo of L4. Rectangle shows the sample location of the thin section in Figure 11A. (C) Core photo of planar laminated to ripple cross-laminated sandstone (L5) showing climbing ripple: Marjorie Campbell No. 1, 9640 ft (2938 m). (D) Core photo of L5 showing planar lamination: Schoenhal No. 1, 8076 ft (2462 m). (E) Photomicrography of L5 showing ripple-cross lamination: Kuhlman No. 3-A, 7990 ft (2436 m). Porosity is 14.9% and permeability is 0.18 md. (F) Photomicrograph showing the contact of L5 and L6. L5 (lower part) is well-cemented and L6 (upper part) has abundant visible Interparticle pores: Kuhlman No. 3-A, 8007.3 ft (2440 m). (G) Core photo showing the contact of L5 and L6. Rectangle shows the sample location of the thin section in Figure 11G.

Lithofacies 6 (L6): Laminated calcareous to siliceous mudstone

Laminated mudstone is the predominant mudstone lithofacies. Dominant mineral content in the laminated mudstone range from siliceous (Figure 12A, B, C, D) to calcareous (Figure 12E). Vertical changes from one sublithofacies to another can be sharp or gradational (Figure 12A). Bedding ranges from very thin to thick laminated. Bioturbation is sparse.

The major grain types range from clay- to silt-size organic-rich peloids, quartz, and fragmented skeletal material (Table 2, Appendix 1). Pyrite and phosphate are present. Pyrite occurs as small framboids aggregates (generally less than 10 um) (Figure 12F) and euhedral crystals. Pyritization of skeletal grains such as cephalopods and bivalves are noted. Silt- to fine-sand-size mud-clasts are common. Much of the original sediment appears to be soft peloids that have been compacted.

Silt- to very fine sand size detrital quartz and feldspar are common. Carbonate content in the siliceous mudstone is probably related to calcareous skeletal material. Calcium is enriched in the intervals that have more calcareous skeletal fragments according to XRF analysis. Other carbonate components in the calcareous mudstones are micrite and peloids. Authigenic minerals include silica, calcite, dolomite, siderite, and pyrite (Table 2, Appendix 1).

Skeletal material consists of echinoderms, radiolarians, sponge spicules, cephalopods, gastropods, brachiopods, trilobites (Figure 12G), bivalves, ostracods (some are rimmed by microcrystalline quartz), foraminifera, and algal macerals. The cephalopods and radiolarians lived in the oxygenated interval of the shallower water column. Organic material is in the form of flakes and disseminated particles and is locally abundant.

Laminations include current ripple laminations and planar laminations. Starved ripples and mud drapes are abundant. Laminations are the result of interlaminated layers of mud and coarser grained material, alternation of mineral types and/or grain types. Laminations may be compacted around coarser rigid grains. Compaction has enhanced laminations in the mudstone (Loucks and Ruppel, 2007). Some laminations are highlighted by alignments of shell fragments, silt grains, mud-clasts and/or organic flakes. Some laminae display millimeter-scale, fining-upward sequences, and others show erosive base or truncation of ripples. Convolute lamination and flame structures are common in the ripple laminated beds. Layers of concentrated, extremely compacted thin shells of skeletal grains (mostly bivalves and brachiopods) are observed at the base of this facies (Figure 12H, I). This facies contains fair to good TOC (Table 3). The laminated siliceous to calcareous mudstone lithofacies can be associated with any of the lithofacies in the Cherokee strata, but is commonly associated with laminated sandstone lithofacies, muddy matrix conglomerate lithofacies, deformed/disorganized mudstone lithofacies, argillaceous mudstone lithofacies, and massive mudstone lithofacies.

Lithofacies 7 (L7): Very thin to thin-laminated argillaceous mudstone

The very thin to thin-laminated argillaceous mudstone lithofacies is characterized by its light gray to dark gray color and appears to be fissile in cores (Figure 12J, K). Burrows and skeletal fragments are extremely rare to nonexistent. Fabric ranges from very thin to thin-wavy lamination. Lamination is enhanced by the alignment of mud-clasts.

Clay-sized detrital quartz and clay minerals are the dominant components in this mudstone lithofacies. Pyrite is also observed. XRD data shows that this lithofacies is clay-mineral rich, and has less than 2.6 wt% carbonates (Table 2, Appendix 1). The low abundance of calcite or dolomite shown in the XRD data corresponds to the extremely low

value of calcium as noted by XRF data and the lack of calcareous skeletal fragments. Illite is relatively abundant (mean: 9.4 wt%) in this lithofacies compared to other mudstone lithofacies (3.9 wt% and 4.6 wt%). This facies has poor to fair TOC (Table 3).

Lithofacies 8 (L8): Massive to faintly laminated siliceous mudstone

Massive to faintly laminated siliceous mudstone (Figure 12L, M) is dark-gray to black color in both core and thin sections. Fabric ranges from nonlaminated to faintly laminated. The faint laminations are related to alignment of mud-clasts and organic flakes. Burrows are extremely rare to nonexistent.

Silt- to clay-size quartz and clay minerals are the dominant minerals. Organic-rich peloid and plagioclase are also present. Authigenic minerals include pyrite, siderite, calcite, and dolomite. Pyrite exists in the form of nodules and layers. Some shell fragments show pyritization. Fossils are rare but include compacted shell fragments, radiolarians, sponge spicules, and agglutinated foraminifera comprised of microcrystalline quartz.

XRD data show that L8 is dominantly composed of quartz, feldspar and clay minerals with minor amounts of calcite, dolomite, gypsum, and ankerite (Table 2, appendix 1). Biogenic silica is probably present and as a product of opal dissolution of sponges and radiolarians (Loucks and Ruppel, 2007). This lithofacies is organic-carbon rich (Table 3).

L8 commonly occurs above the laminated mudstone lithofacies. It has a greater thickness in the more distally located Marjorie Campbell No. 1 core than in the more proximal located Kuhlman No. 3-A core.

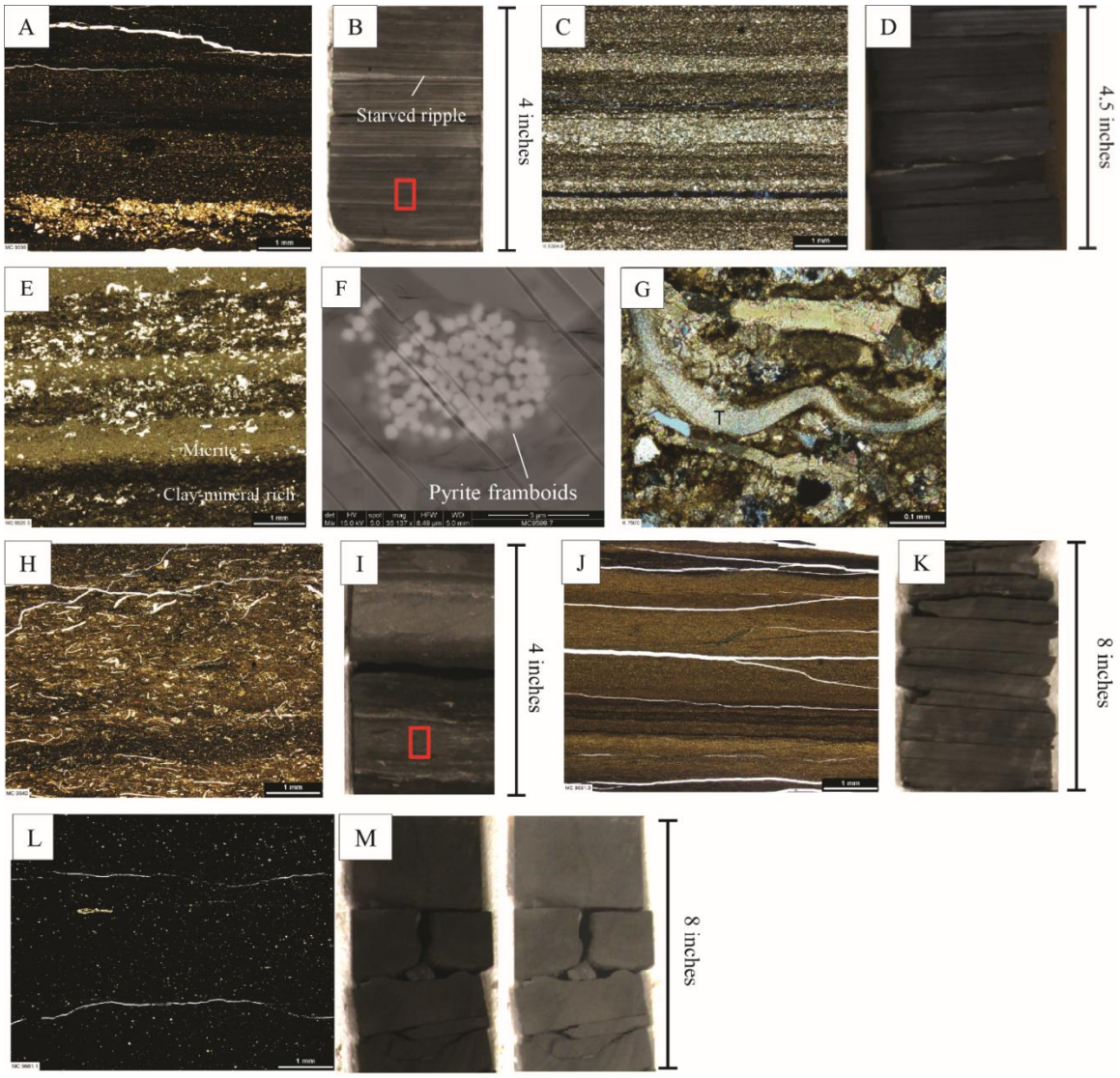
A
B
Starved ripple
4 inches
C
D
4.5 inches
E
Micrite
Clay-mineral rich
F
Pyrite framboids
G
T
H
I
4 inches
J
K
8 inches
L
M
8 inches

Figure 12

Figure 12. Photographs of mudstone lithofacies (L6, L7, and L8). (A) Photomicrograph of laminated siliceous mudstone lithofacies (L6): Marjorie Campbell No. 1, 9559 ft (2914 m). TOC is 2.18 wt%. (B) Core photo of L6. Rectangle shows the sample location of the thin section in Figure 12A. (C) Photomicrograph of laminated siliceous mudstone lithofacies (L6): K 8954.8 ft (3004 m). TOC is 0.84 wt%. (D) Core photo of L6. Rectangle shows the sample location of the thin section in Figure 12C. (E) Photomicrograph of laminated calcareous mudstone lithofacies (L6): Marjorie Campbell No. 1, 9820 ft (2993 m). (F) SEM image showing pyrite framboids and intraparticle pores between the pyrite framboid aggregates: Marjorie Campbell No. 1, 9599.7 ft (2926 m). (G) Photomicrograph showing a trilobite (T): Kuhlman No. 3-A, 7979 ft (2932 m). (H) Photomicrograph Layers of strongly compacted skeletal fragments within laminated mudstone lithofacies (L6): Marjorie Campbell No. 1, 9762.4 ft (2976 m). (I) Core photo showing the layers of strongly compacted skeletal fragments with erosive base: Marjorie Campbell No. 1, 9840 ft (2999 m). (I) Photomicrograph of erosive base presents on the base of compacted skeletal fragment deposits. (J) Photomicrograph of Laminae in very thin to thin-laminated argillaceous mudstone (L7): Kuhlman No. 3-A, 8054.8 ft (2455 m). TOC is 0.84 wt%. (K) Cores are split along the horizontal planes. (L) Photomicrograph of massive to faintly laminated siliceous mudstone (L8): Marjorie Campbell No. 1, 9801 ft (2987 m). TOC is 6.77 wt%. (M) Core photo showing L8 is dark in color and appears to be massive or faintly laminated with enhanced light (core on the right).

Lithofacies 9 (L9): Disturbed and disorganized mudstone

The mineral and grain composition of the disturbed and disorganized mudstone (Figure 13A) is similar to the laminated siliceous to calcareous mudstone lithofacies. Convolute laminations, over-turned cross-laminations (Figure 13B, C), disrupted laminations, flame structures, contorted laminations, and/or microfaults (Figure 13B) are evidence for the disruption and lack of organization. Water-escape structures are also present.

Lithofacies 10 (L10): Grainstone and grain-dominated packstone

Grainstone and grain-dominated packstone lithofacies (Figure 13D, E) is a group of grain-supported carbonate rocks, which contain minor or no mud matrix. Grain types and sizes vary by layers. Nonskeletal grains include ooids (cerebroid and radial), oncoids, cortoids, and peloids. Skeletal grains consist of rugose and tabulate corals, crinoids, ostracods, bivalves, brachiopods, trilobites, and bryozoans. Siliciclastic grains (silt-size quartz and feldspar) are present in grain-dominated packstone.

Lithofacies 11 (L11): Peloidal packstone

The peloidal packstone lithofacies (Figure 13F, G) consists of silt- to fine-sand size peloids within mud matrix. This lithofacies has low porosity and permeability (Porosity ranges 0.1%-10.2%, permeability ranges less than 0.001 to 0.058 md). Some of the peloids were probably fecal pellets formed in shallower water and transported into or settled by suspension in the deeper basin (Loucks and Ruppel, 2007). Other peloids may have been produced by flocculation of clay particles (marine snow), which later settled to the sea bottom (Loucks and Ruppel, 2007; Schieber, 2010).

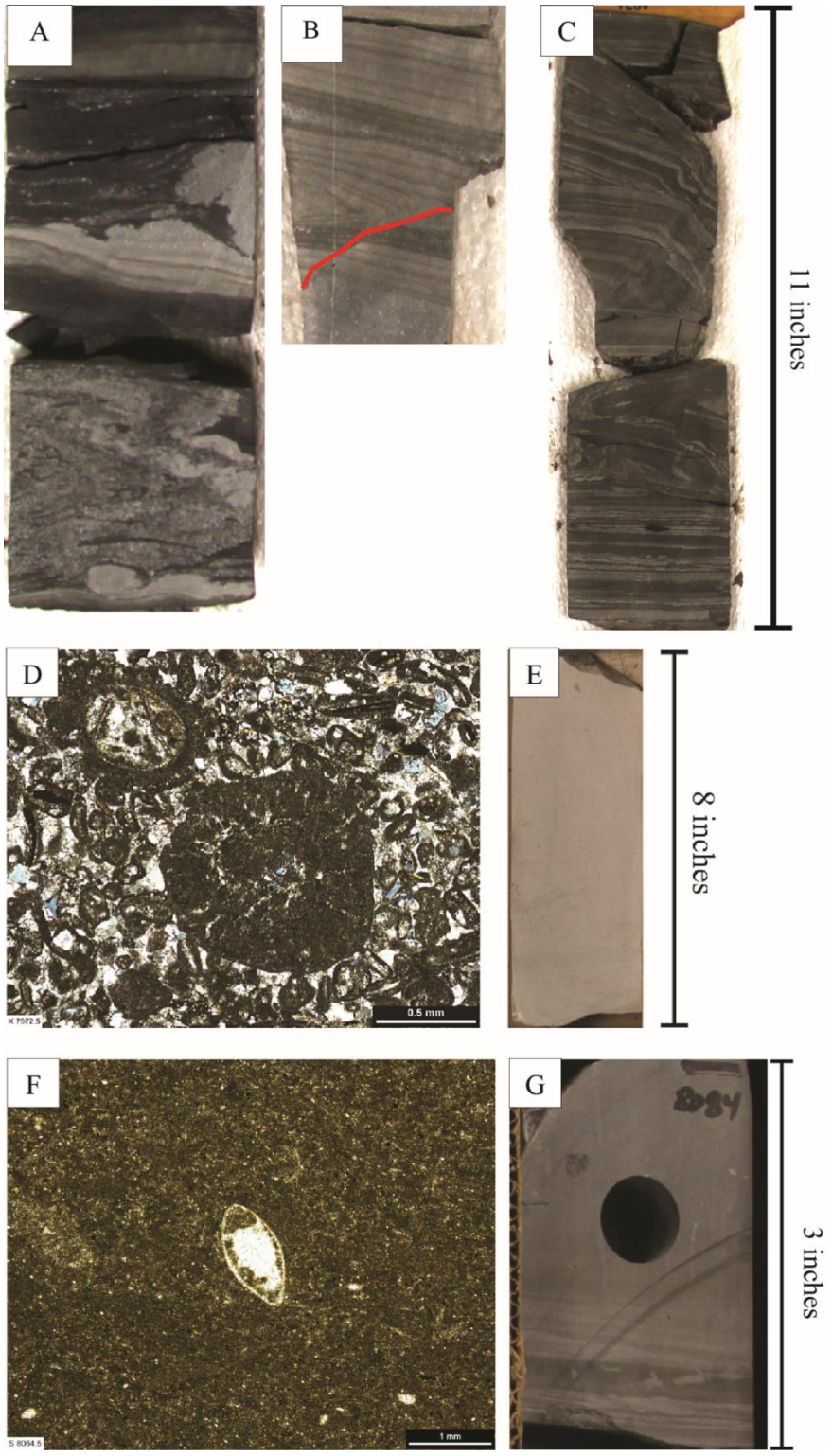

Figure 13

Figure 13. Photographs of disorganized and/or disturbed laminated mudstone (L9) and carbonates (L10 and L11). (A) Disorganized mudstone (L9): Marjorie Campbell No. 1, 9640 ft (2938 m). (B) Overturned laminated mudstone (L9) with micro-fault: Marjorie Campbell No. 1, 9609 ft (2929 m). (C) Overturned laminated mudstone (L9): Marjorie Campbell No. 1, 9609 ft (2929 m). (D) Oolitic grainstone (L10): Kuhlman No. 3-A, 7972.5 ft (2430 m). Porosity is 3.1% and permeability is 0.027 md. (E) Oolitic grainstone with no sedimentary structures visible. (F) Peloidal mud-dominated packstone (L11): Schoenhal No. 1, 8084.5 ft (2464 m). Porosity is 1.1% and permeability is less than 0.001 md. (G) Peloidal mud-dominated packstone showing fine laminations.

Table 2. Mineralogical Analysis of the Cherokee Group Based on XRD Data

	Laminated calcareous to siliceous mudstone		Very thin to thin-laminated argillaceous mudstone		Massive to faintly laminated siliceous mudstone		Peloidal packstone	
	Mean (wt%)	Percent (%)	Mean (wt%)	Percent (%)	Mean (wt%)	Percent (%)	Mean (wt%)	Percent (%)
Quartz	9.93	29.27	9.08	30.11	9.82	30.66	5.33	14.96
K-Feldspar	1.31	3.86	1.16	3.85	0.98	3.05	0.46	1.29
Plagioclase	3.33	9.82	2.50	8.28	3.40	10.60	1.63	4.59
Fe-Calcite	0.00	0.00	0.00	0.00	1.88	5.87	0.00	0.00
Calcite	6.38	18.81	1.16	3.83	5.13	16.01	3.42	9.61
Aragonite	1.26	3.71	0.00	0.00	0.00	0.00	0.00	0.00
Fe-Dolomite	5.09	15.01	0.16	0.53	2.16	6.73	18.30	51.37
Dolomite	0.00	0.00	0.00	0.00	1.06	3.32	0.00	0.00
Siderite	0.08	0.24	0.82	2.74	0.18	0.55	0.00	0.00
Pyrite	0.28	0.83	0.85	2.82	0.71	2.23	0.48	1.36
Apatite	0.22	0.65	0.00	0.00	0.00	0.00	0.00	0.00
Gypsum	0.11	0.32	0.45	1.50	0.17	0.54	0.00	0.00
Natrojarosite	0.00	0.00	1.69	5.60	0.17	0.54	2.90	8.14
Illite&Mica	3.86	11.38	9.41	31.21	4.62	14.42	2.36	6.62
Kaolinite	0.65	1.92	0.95	3.15	0.66	2.06	0.23	0.65
Chlorite	1.42	4.19	1.93	6.40	1.10	3.43	0.51	1.43
Clay minerals	5.93	18.29	12.29	46.65	6.38	21.13	3.10	9.61
Quartz and Feldspar	14.56	44.92	12.74	48.35	14.20	47.05	7.43	23.02
Calcite and Dolomite	11.93	36.80	1.32	5.00	9.60	31.82	21.72	67.36

	Grainstone and grain-dominated packstone		Planar laminated to ripple cross-laminated sandstone		Massive sandstone		Muddy matrix conglomerate	
	Mean (wt%)	Percent (%)	Percent (%)	Percent (%)	Mean (wt%)	Percent (%)	Mean (wt%)	Percent (%)
Quartz	2.08	5.08	11.98	28.03	10.40	28.42	9.47	25.53

Table 2 (continued)

K-Feldspar	0.26	0.64	1.73	4.04	3.95	10.79	3.05	8.23
Plagioclase	1.09	2.67	5.20	12.16	12.50	34.14	10.71	28.87
Fe-Calcite	3.62	8.85	6.08	14.24	0.00	0.00	1.75	4.70
Calcite	20.62	50.39	7.87	18.40	1.73	4.73	2.74	7.38
Aragonite	2.40	5.86	5.09	11.90	0.00	0.00	0.00	0.00
Fe-Dolomite	3.49	8.53	1.22	2.86	4.39	11.99	2.99	8.07
Dolomite	6.26	15.30	0.36	0.84	0.00	0.00	1.18	3.18
Siderite	0.02	0.04	0.07	0.16	0.00	0.00	0.00	0.00
Pyrite	0.04	0.09	0.08	0.19	0.11	0.31	0.26	0.71
Apatite	0.13	0.32	0.83	1.95	0.00	0.00	0.00	0.00
Gypsum	0.00	0.00	0.00	0.00	0.00	0.00	0.00	0.00
Natrojarosite	0.08	0.20	0.00	0.00	0.00	0.00	0.00	0.00
Illite&Mica	0.75	1.82	1.60	3.74	1.21	3.31	1.67	4.49
Kaolinite	0.03	0.08	0.21	0.48	0.42	1.16	1.04	2.81
Chlorite	0.06	0.14	0.43	1.00	1.89	5.16	2.24	6.04
Clay minerals	0.84	2.27	2.43	6.50	3.52	9.66	5.21	14.61
Quartz and Feldspar	3.43	9.30	20.19	54.12	26.84	73.58	23.23	65.20
Calcite and Dolomite	32.64	88.44	14.69	39.38	6.12	16.77	7.19	20.19

LITHOFACIES ASSOCIATIONS

Lithofacies association 1 (FA1): Amalgamated thick-bedded turbidites and debris-flow/mud-flow deposits

Description

Lithofacies association 1(FA1) (Figure 14A) consists of upward fining sedimentary packages up to 6 m thick, composed of basal conglomerates (L1, L2, and/or L3) overlain by massive sandstones (L4) and planar to cross-laminated sandstones (L5) or transported grainstone or grain-dominated packstones (L10). Disorganized and/or disturbed laminated mudstones (L9) can also be present at the top of the section replacing the sandstone beds. It is commonly associated with the muddy matrix conglomerates (L2). Basal conglomeratic units of this lithofacies association are characterized by sharp bases and abundant mudstone rip-up clasts; thin inversely graded layers are sometimes overlying the lower contact. Upward through the FA1, individual beds generally exhibit less evidence of erosion (e.g., mud-clasts and sharp erosive surfaces on the base of sandstone beds). Amalgamation of packages of sandstones is common. Composite intervals of FA1 strata can be associated with thick successions of FA2 (upward thinning beds of upward fining turbidites) or FA3 (hemipelagic suspension and muddy turbidite deposits). This lithofacies association is characterized by blocky (constant low GR bounded by high GR on top and base) or upward fining (increasing GR) pattern on wireline-logs (Figure 14A). FA1 is the dominated lithofacies association in Flower Thrust No. 3-8. Kuhlman No. 3-A and Sam Hill No. 2-A also contain this lithofacies association.

Interpretation

Deposits of FA1 record the waning of gravity flows as they passed through a location (Mutti and Normark, 1987; Hubbard et al., 2009). The basal conglomerate units were deposited by debris flow (L2) and high-density turbidity currents (L3). The gravity flows were erosive as evidenced by mud rip-up clasts. The subsequence thick- to thin-bedded turbidites were deposited as high- (L4) to low-density turbidity currents (L4, L5). In some cases, turbidite sandstone beds were replaced by the disorganized/disturbed mudstone beds (L9) associated with slumping of fine-grained sediments. The interpretations for the depositional settings are: (A) progressive channel abandonment or the deposition of migrating submarine channel sediments (Bouma et al., 1985c; Stow et al., 1985; Mutti and Normark 1987; Hubbard et al., 2009), and/or (B) sand-rich lobes deposited in erosional settings (Normark et al., 1993). The origin of the upward fining sequence FA1 is difficult to confirm because of the limited lateral viewing area of core. Three-dimensional-seismic data from the adjacent Custer, Blaine, and Caddo Counties in Oklahoma show channel lateral accretion in the Cherokee Group (Lambert, 2006). Similar channel migration processes may have occurred in this study area.

Lithofacies association 2 (FA2): Upward fining and thinning sandstone/carbonate turbidites

Description

Lithofacies association 2 (FA2) is composed of massive sandstones (L4) overlain by planar to cross-laminated sandstones (L5) or carbonates (L10 and L11) and ripple laminated siliceous to calcareous mudstones (L6) (Figure 14B). The sandstone beds show upward thinning and fining. Water-escape structures are observed in some of the massive sandstone units (L4). The massive sandstones are absence in some areas. The bases of FA2 are locally associated with disrupted laminated mudstone units (L9). Scours and rip-up

clasts are locally present at the base of massive sandstone beds, but the size of mud-clasts (fine to very coarse-sand size) are generally smaller than they are in the FA1 (up to pebble-size). FA2 is commonly overlain by deposits of FA3 and underlain by deposits of FA1. This lithofacies association shows upward fining (increasing GR) pattern on wireline-logs. FA2 occurs in Marjorie Campbell No. 1, Sam Hill No. 2-A, Schoenhal No. 1, and Kuhlman No. 3-A wells.

Interpretation

The lithofacies association 2 was deposited by turbidity currents. The vertical lithofacies stacking pattern can be interpreted as levee/overbank deposits (Normark et al., 1993; Hubbard et al., 2009). Disorganized mudstone beds (L9) at the base of FA2 record slumping of the channel levee. Overlying massive sandstone units (L4) were deposited from suspension sedimentation associated with high-density turbidity currents, and capped by spilled-over laminated mudstone deposits by low-density turbidity currents when the sediment-gravity flows within the levees spread into out-of-channel areas (Manley et al., 1997, Hubbard et al., 2009). An alternate interpretation of this lithofacies association is distal fringe of fan deposits (Normark et al., 1993; Hickson and Lowe, 2002; Kane and Pontén 2012). It is difficult to distinguish between levee deposits and fan units (Hickson and Lowe, 2002), especially using core. According to the sand-body geometry that was identified from gross-sandstone isopachous maps, both of the two interpretations may be valid for the deep-water system.

Lithofacies association 3 (FA3): Hemipelagic suspension and muddy turbidite deposits

Description

Lithofacies association 3 is composed of laminated calcareous to siliceous mudstones (L6) and/or very thin to thin-laminated argillaceous mudstones (L7), and massive to faintly-laminated siliceous mudstones (L8) (Figure 14B). Laminated mudstones (L6) may be bioturbated, especially when it is associated turbiditic sandstones (L5). This lithofacies association shows an vertical irregular trend and has high GR on wireline-log responses. FA3 occurs in all studied wells except for Rio Bravo No. 2 well.

Interpretation

Lithofacies association 3 represents "background" sedimentation in a deep-water system. When FA3 is associated with FA2 or FA1, it shows construction from gravity flow events, such as construction of the fine-grained tops of turbidity currents that spilled over the banks of channels (Hubbard et al., 2009)

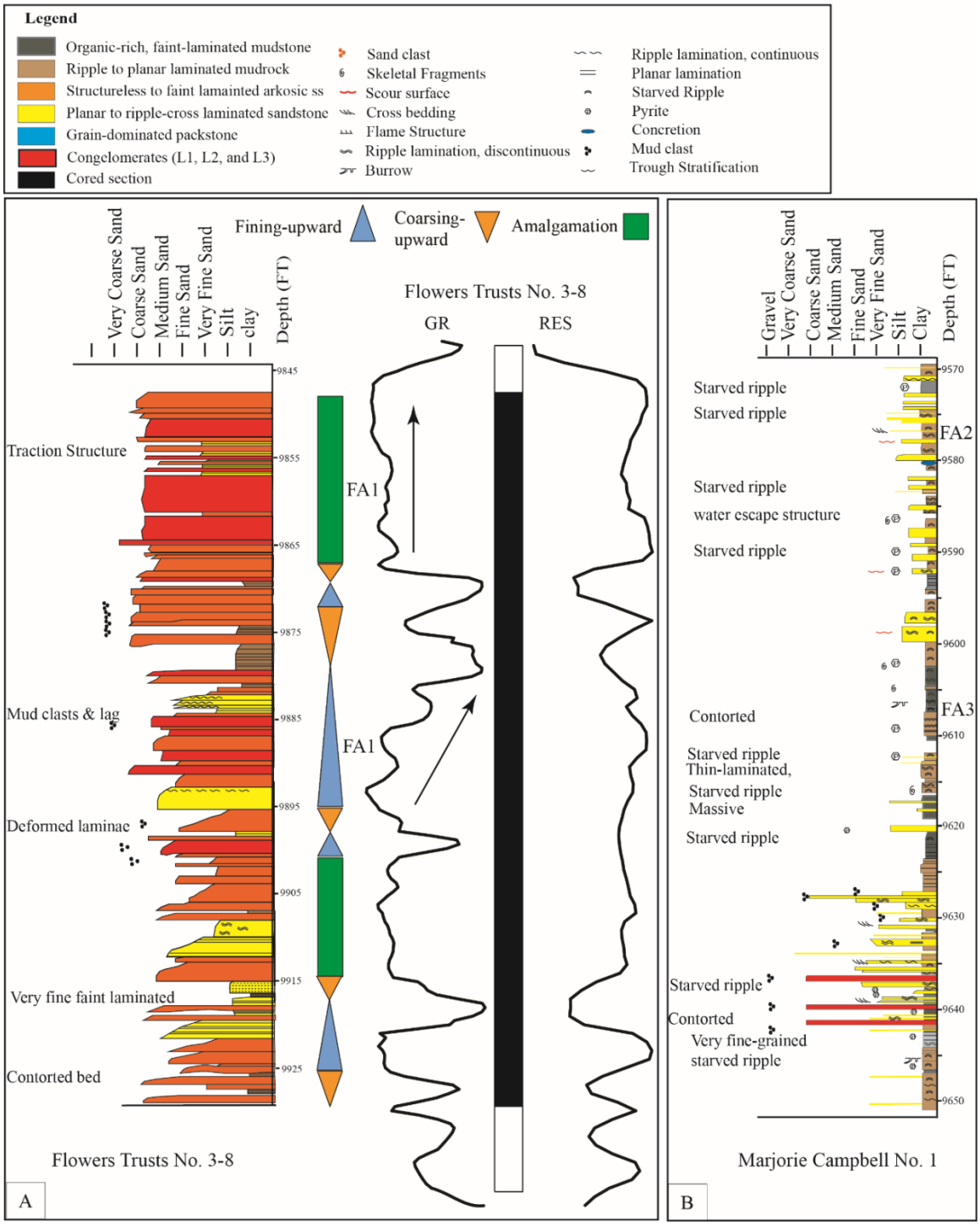
Legend
Organic-rich, faint-laminated mudstone
Ripple to planar laminated mudrock
Structureless to faint lamainted arkosic ss
Planar to ripple-cross laminated sandstone
Grain-dominated packstone
Congelomerates (L1, L2, and L3)
Cored section
Sand clast
Skeletal Fragments
Scour surface
Cross bedding
Flame Structure
Ripple lamination, discontinuous
Burrow
Ripple lamination, continuous
Planar lamination
Starved Ripple
Pyrite
Concretion
Mud clast
Trough Stratification
Fining-upward
Coarsing-upward
Amalgamation
Very Coarse Sand
Coarse Sand
Medium Sand
Fine Sand
Very Fine Sand
Silt
clay
Depth (FT)
Flowers Trusts No. 3-8
GR
RES
9845
9855
9865
9875
9885
9895
9905
9915
9925
Traction Structure
Mud clasts & lag
Deformed laminae
Very fine faint laminated
Contorted bed
FA1
FA1
Flowers Trusts No. 3-8
A
Gravel
Very Coarse Sand
Coarse Sand
Medium Sand
Fine Sand
Very Fine Sand
Silt
Clay
Depth (FT)
9570
9580
9590
9600
9610
9620
9630
9640
9650
Starved ripple
Starved ripple
FA2
Starved ripple
water escape structure
Starved ripple
Contorted
FA3
Starved ripple
Thin-laminated,
Starved ripple
Massive
Starved ripple
Starved ripple
Contorted
Very fine-grained
starved ripple
Marjorie Campbell No. 1
B

Figure 14

Figure 14. Core descriptions of Flowers Trusts No. 3-8 (A) and Marjorie Campbell No. 1 (B) showing lithofacies association 1, 2, and 3. Although both of the two wells show upward-fining patterns, coarse-grained sediment beds in Flowers Thrust well are thicker and coarser than they are in Marjorie Campbell No. 1. The amalgamated sandstones and conglomerates in the Flowers Thrusts No. 3-8 are interpreted to be proximal lobe or amalgamated channel-fill deposits. The sandstone beds in Marjorie Campbell No. 1 are interpreted to be distal lobe or channel-levee deposits that were deposited by turbidity currents. See well locations on Figure 1.

REGIONAL STRATIGRAPHIC FRAMEWORK

Hendrickson et al. (2001) published type-wireline logs of the Cherokee Group on the shelf and basin areas and on the Wichita-Amarillo Mountain front. They suggested that the "Cherokee marker", "Pink limestone marker", and the top of Atoka Group can be correlated throughout the Anadarko Basin (Hendrickson et al., 2001). However, all type wireline-logs are located in Oklahoma and no cross-sections from the Texas Panhandle were shown in their paper. Investigations have been conducted to illustrate the productive sandstones of the Cabaniss Group (Upper Cherokee Group; figure 2) (e.g., Puckette, 1990) and the underlying Krebs Group (Lower Cherokee Group; Figure 2) (e.g., Anderson, 1992; Johnson, 1984) in the Anadarko Basin area in Oklahoma (Beckham, Dewey, Custer, Ellis, Roger Mills, Washita, Caddo, and Blaine Counties). Correlation of type wireline-logs from Oklahoma to the study area was attempted in this investigation. However, because of local lithologic and thickness changes, variation on wireline-log signatures and insufficient well control between previous study area and current study area, the correlations were difficult and may be imprecise. The limestone marker beds that were used on the shelf are not widespread and are difficult to recognize on wireline logs in the deep-water slope to basin setting. Puckette (1990) documented similar issues about the shelf to basin correlations of the Cabaniss Group in Oklahoma. The markers for wireline-log correlations in Oklahoma are not adaptable to this study. A new stratigraphic framework in the study area was established and discussed (Figure 2).

The basal Cherokee contact with the Atoka is defined as the base of a regional continuous high-gamma-ray, shale-marker bed that overlies a low-gamma-ray limestone bed. This contact matches with the contact suggested by Hendrickson et al. (2001). The top of the Cherokee Group is defined as the base of Oswego Limestone (Hentz 2011; Higley,

2014). The wireline-log response of Oswego Limestone is generally blocky, but it may also contain several upward coarsening or upward fining limestone units. Identification of the Oswego Limestone is based on the cross sections published by Hentz (2011). Within the Cherokee Formation, four flooding surfaces mark major, regionally persistent changes from a lower transgressive succession with a consistently upward-finning GR-log signature to a regressive succession with an upward-coarsing GR-log signature (Figure 2). The flooding surfaces may record the shut-down of sediment supply. Flooding surface 3 (FS3) coincide with the "Cherokee marker" that marks top of Verdigris Limestone bed suggested by Hendrickson et al. (2001), marking a regional transgression event possibly controlled by glacial eustasy. Flooding surfaces 1 and 2 extend across the study area. FS 3 pinches out to the west of the study area. FS 4 and FS 5 pinch out to both west and northeast. The five depositional packages are bounded by the flooding surfaces (Figures 2, 9).

The Cherokee interval thickens significantly from north to east across the study area (Figures 8, 9). The gross sandstone isopachous maps of depositional packages with the lithofacies allow the delineation of the spatial and temporal evolution of the slope to basin-floor system (Figure 15). Package 1 (bounded by Cherokee base and flooding surface 1) ranges from less than 100 ft (30 m) to more than 1500 ft (457 m) thick. Package 1 thickens from north to east of the study area. Lobate-elongate geometries are recognized on gross sandstone isopachous map (Figure 15A). Lobe complexes are oriented from south to north in the Hemphill and Robert Counties, from west to east in the Ochiltree County, and from north to south in the Lipscomb County.

Package 2 ranges from less than 50 ft (15 m) to more than 700 ft (213 m) thick. Lobe-elongate geometries are also observed on the gross sandstone isopachous map (Figure 15B), but the orientation of the lobe complex at the Ochiltree County shifted to the north. Coarse-grained sediments were mainly delivered by the channel-lobe complexes on

the south of study area. Several wells (Kuhlman No. 3-A and Flower Thrust No. 3) contain proximal lobe or channel-fill deposits (FA1) and are located at the axis and fringe of the lobe complexes. The Marjorie Campbell No. 1 and Schoenhal No. 1 wells that are dominantly composed of channel-levee or distal lobe deposits (FA2) are located at the distal part of lobe complex.

Package 3 (Figure 15C) is approximately 27 ft (8 m) to 550 ft (168 m) thick. Thick sandstone accumulations appear at the edge of the wireline-log dataset as shown by the gross sandstone isopachous map (Figure 15D) and may be artifacts related to the lack of data control near the edge. Lobe geometries in the southern study area are similar with the sand-body geometries observed in Package 1 and Package 2. Although no cores are available for Package 3, the depositional setting is probably similar to Package 1 and Package 2. Package 4 (Figure 15D) is approximately 17 ft (5 m) to 700 ft (213 m) thick. The sandstone bodies exhibit more elongated geometry compared to Package 1 to 3 and concentrated to the northeast of the study area. The elongated geometry may indicate a mud to sand-rich slope ramp (Reading and Richard, 1994). Package 5 (Figure 15E) is up to 300 ft (91 m) and shows an isolated sand-body geometry. The sand-body geometry of Package 5 has similar trend with the overlaying Oswego Limestone, and may be related to the formation of a local carbonate buildup. The rapid decrease in thickness of the depositional Package 4 and Package 5 and the pinch-outs of the flooding surfaces 3 and 4 to the northern most part of the study area indicate a possible paleohigh controlled by regional structures (Hentz, 2011). Additional core data is needed to better understand the observed sand-body geometry of Package 3, 4 and 5.

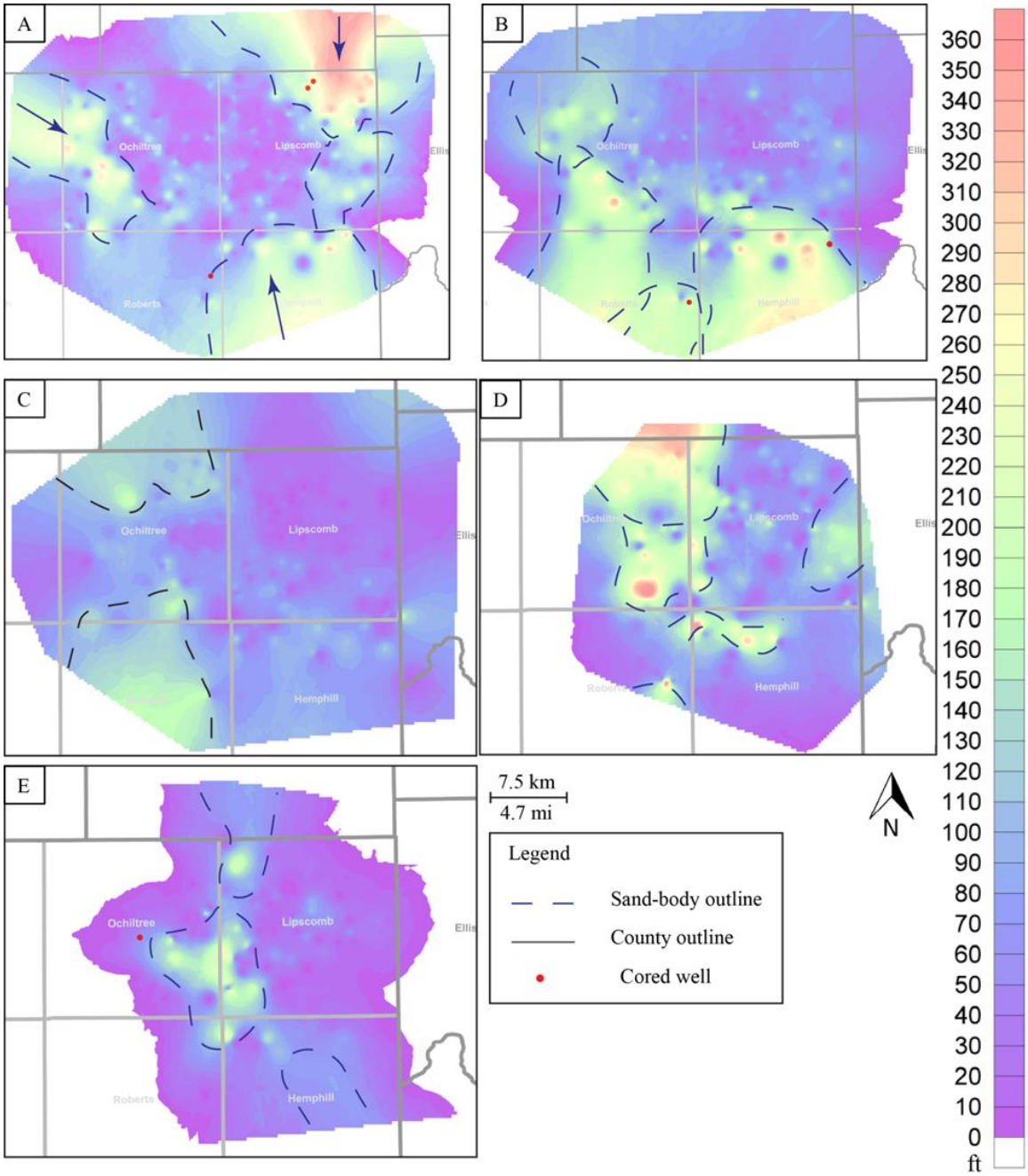

Figure 15. Gross-sandstone thickness maps of the five depositional packages in the Cherokee Group. Red plots showing cored well locations. (A) Package 1. (B) Package 2. (C) Package 3. (D) Package 4. (E) Package 5.

DEPOSITIONAL MODEL AND DISCUSSION OF DEPOSITIONAL PROCESSES

On the basis of sedimentary structures, lithofacies, biota, organic and inorganic geochemistry, sandstone isopachous maps, and comparisons with regional sedimentological and tectonic features, a depositional model that explains depositional processes and products observed in the Cherokee Group in the study area is proposed (Figure 16). The Cherokee depositional lithofacies in the study area are most appropriately interpreted as having formed in a deep-water slope to basinal setting. The basin was characterized by dysoxic to anoxic bottom conditions developed below storm-wave base and below the oxygen-minimum zone. Sedimentation in the basin was primarily the result of two processes: suspension settling and gravity flows. Sediments were possibly later reworked by bottom currents. Sediments were fed to the basin floor by fan delta systems to the south and by fluvial-deltaic systems from a mix siliciclastic-carbonate shelf to the north (Higley, 2014). Although allochems are common in the Cherokee basinal strata, they are interpreted to be dominantly transported from adjacent shelves and upper-slope settings.

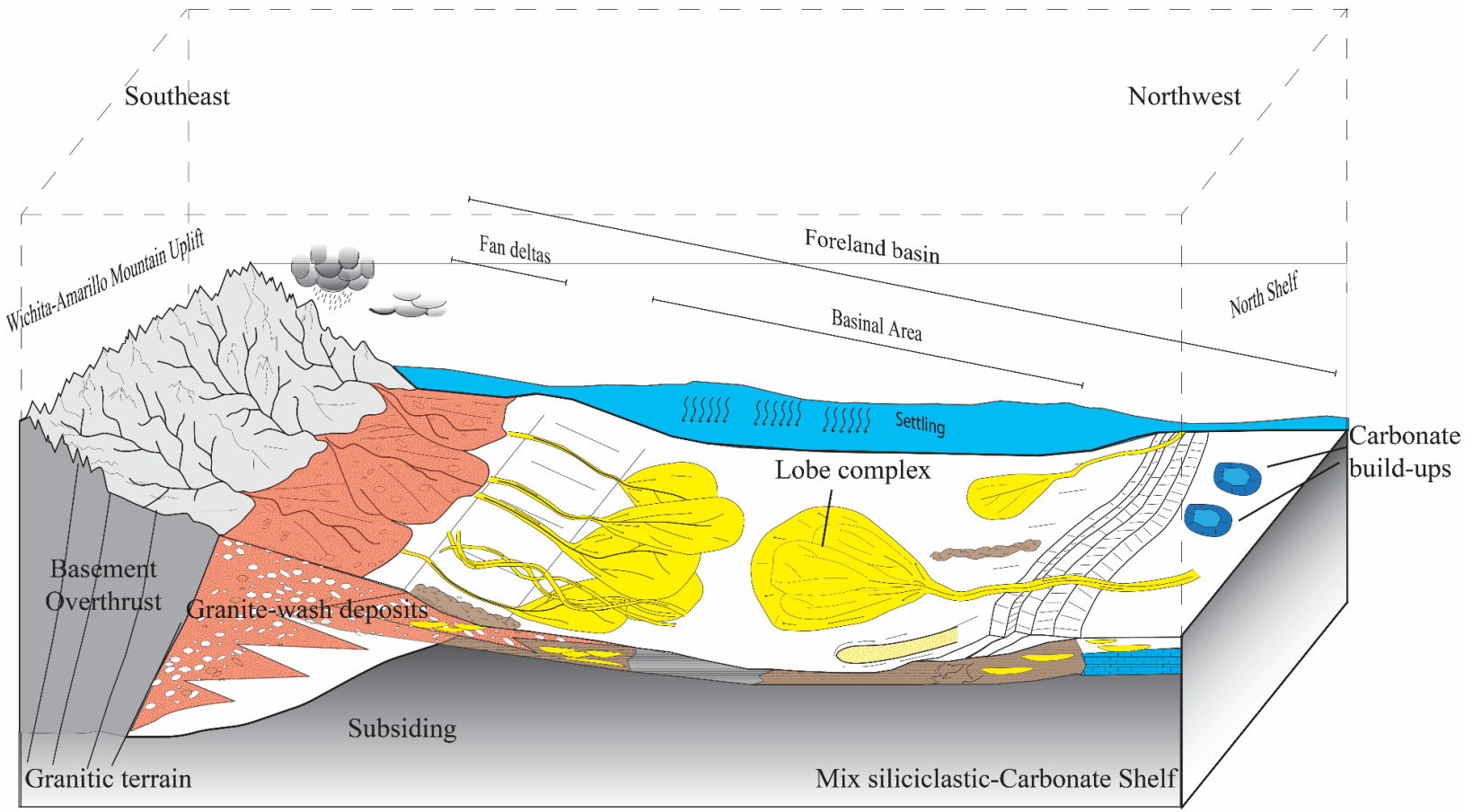

Figure 16. Generalized depositional model for the Cherokee Group in Texas Panhandle showing sediment sources, depositional processes, and depositional environment. Model modified from Reading and Richards (1994), Sinclair and Naylor (2012), and Sorenson (2005).

SEDIMENT SOURCE

Two major sediment sources are identified in study area. The Kansas Shelf to the north contributed carbonate debris and siliciclastic sediments. The Wichita-Amarillo Mountain uplift to the south was another source area for siliciclastic sediments. These siliciclastic sediments contain significant amounts of K-feldspars with perthitic structures and metamorphic and granitic rock fragments that are similar to those observed in the Wichita Mountains (Merritt, 1964; Ham and Wilson, 1967). Previous studies in Oklahoma documented similar observations (Hansen, 1978; Puckett, 1990; Johnson, 1984; Udayashankar, 1985; Anderson, 1992). A ternary diagram (Figure 3C) constructed from XRD data shows differences in mineral composition of coarse-grained sediments from the two sediment sources. Coarse-grained sediments in core in the north contain more carbonate minerals, while coarse-grained sediments in cores in the south are rich in feldspars (more than 30 wt%). Sediments that are interpreted to be sourced by the Wichita-Amarillo Mountain uplift show poor textural maturity (poorly to moderately sorted, angular to subrounded shape, and are coarse grained (up to pebble size), suggesting short transport distance. Siliciclastic sediments that are interpreted to having been sourced from the north shelf display better textual maturity and are finer grained (very fine to fine-sand size).

The sediment transport directions can be inferred by the orientation of the gross-sandstone geometries (Figure 15A-E). Three sediment transport directions are identified in Package 1 according to the elongate-lobate sand-body geometry: south, north, and west. The first two directions coincide with the interpretation of the two dominant source areas. The third sediment transport direction indicates a possible sediment source from the Cimarron Arch (Figure 15A) (Hentz, 2011). Coarse-grained sediments in Package 2 and 3

were derived from the south. At the time depositing Package 4, the sediments were dominantly derived from the north.

DEPOSITIONAL SETTING

Deposition of the Cherokee Group in study area was in deep-water, below storm-wave base setting. Deposition of sediments was predominately by gravity flows and hemiplagic settling. No diagnostic evidence exists that sediments were reworked by shallow-water processes (such as wave- or tide-induced sedimentary structures). The mixture of fauna living in different environment indicates that the shallower water fauna was transported into the deeper water.

Two hypotheses relative to depositional setting of the Cherokee Group were made in an area (Beckham, Dewey, Custer, Ellis, Roger Mills, Washita, Caddo, and Blaine Counties in Oklahoma) adjacent to the study area. The depositional setting of the Red Fork sandstones in Krebs Group (Figure 2) were described as submarine fans in deep water setting (Whiting, 1982; Johnson, 1985; Anderson, 1992). Skinner sandstones in Cabaniss Group (Figure 2) were interpreted to be deposited in a fluvial-deltaic shallow-marine depositional environment (Johnson 1985; Puckett, 1990) in the same area. Evidence provided for the interpretation of a shallow-marine depositional setting includes: 1) a possible caliche horizon that indicates subaerial exposure (Puckett, 1990), 2) interpreted shallow-water brachiopod fossils in the studied core (Johnson, 1985), 3) the presence of lenticular beddings (Johnson, 1985), and 4) the hinge line suggesting a shelf break as proposed by Johnson (1985). In the study area, no caliche or other evidence that suggest subaerial exposure were observed in the cores. Major depositional processes inferred from the Cherokee lithofacies and sedimentary structures are suspension settling, turbidity currents, debris flows, and bottom currents. Similar down-dip thickening trends described

by Johnson (1985) were observed in the study area, but evidence of the hinge line is not present in the study area as the change on slope angle is subtle (estimated change on slope angle from structure contour map [Figure 6] is less than 0.01^0). The paleogeography map of early Desmoinesian by Rascoe and Adeler (1983) supports this interpretation.

DEPOSITIONAL PROCESSES

Coarse-grained sediments (both siliciclastic and carbonate) were transported into the basin by sediment gravity flows. To the north of Wichita-Amarillo Mountain uplift, the deposition of conglomerates and coarse-grained sands was by debris flows and high-density turbidity currents in confined channel and proximal-middle fan settings. Turbidites were deposited when the system became less confined. Similar examples were documented in other foreland basin deep-water systems (Hickson and Lowe, 2002; Hubbard et al., 2009). In the north of the study area, deposition of sandstones and carbonates were predominately by turbidity currents.

The conglomeratic facies (L1, L2, and L3) are only observed in the wells to the just north of Wichita-Amarillo Mountain uplift on the southern side of the basin (Marjorie Campbell No.1 and Flower Thrust No. 3-8). Mud-clast conglomerate lithofacies (L1) are developed in areas associated with erosion of underlying sediments, including the bases of channels and scours. The abundance, large grain size, and angular shape of mud-clasts suggest a short transport distance. The mud-clasts were derived from local erosion of the sea floor probably just a short distance upslope from the area of deposition (Masalimova, 2013). This lithofacies is interpreted to have been deposited at the base of confined channels. Two process-based interpretations are possible for the deposition of mud-clasts in a sand matrix. One interpretation is that deposition occurred as a result of high-density turbidity currents as described by Lowe (1982) and Talling (2012). Another interpretation

is that deposition resulted from a higher cohesive strength debris flows as the DM-2 facies presented by Talling (2012). Mud-clasts deposited though this processes are chaotically distributed (Talling, 2012). However, the mud-clasts in the studied cores show alignment. Together with the predominance of a moderately to well-sorted sand matrix, the deposition of L1 is interpreted as high-density turbidity currents. The sandy siliciclastic conglomerate facies (L2) is interpreted to be deposited by gravel-bearing high-density turbidity currents as defined by Lowe (1982). What appears to be muddy matrix between rigid grains are actually compacted mud-clasts (pseudomatrix). The muddy matrix conglomerate lithofacies (L3) was deposited as a result of en-mass freezing of a cohesive debris flow (Lowe, 1982; Talling et al., 2012). This interpretation is based on the lack of internal sedimentary structures and the presence of large clasts within a muddy matrix. The larger clasts are supported by the buoyancy and strength and viscosity of the clay-water matrix (Lowe, 1982). Deposition occurred when the driving gravitational stress decreased below the strength of the flow (Middleton and Hampton, 1973).

Sandstone lithofacies (L4, L5) are present in all studied cores except for the Rio Bravo No. 2 core. Differences in the massive sandstone that was deposited by high-density turbidity currents and by debris flows were discussed by Talling (2012). Although it is difficult to differentiate massive sandstones deposited by these two different processes using one-dimensional observations in core, Talling (2012) summarized characteristics of the massive sandstones deposited by debris flow as: 1) containing chaotically distributed clasts, 2) showing grain-size breaks that mark the upper boundary, and 3) having a relatively flat base. These characteristics are not observed in the studied cores. The massive sandstones lithofacies (L4) is interpreted to be deposited by sandy high-density turbidity currents as described by Lowe (1982). Deposition was by direct suspension sedimentation (Walker, 1978) when suspended-load fallout rate is rapid such that the sediment has

insufficient time for development of either a bedload layer or an organized traction carpet (A division of Bouma, 1962; S_3 division of Lowe, 1982). The resulting deposits are grain-supported and lack traction structures. Water-escape structures that were developed during mass settling, such as dish structures, are consistent with the inferred rapid sedimentation and show that the deposits underwent liquefaction or post-depositional disturbance (Lowe, 1975). Abundance of angular to subrounded mud rip-up clasts, scours, and amalgamation surfaces are also consistent with the interpretation of energetic and locally erosive currents. Planar laminated sandstone beds (L5) are interpreted to be deposited by low- (Tb division of Bouma, 1962) to high-density (S2 division of Lowe, 1982) turbidity currents. Ripple cross-laminated sandstone beds (L5) were deposited from a relatively dilute and fully turbulent suspension, with relatively low rates of sediment fallout (Tc Division of Bouma, 1962; Talling 2012). The presence of climbing ripple suggests a combination of traction (to form ripples) and rapid fall-out of sediment from suspension (Middleton and Hampton, 1973)

The grainstone and grain-dominated packstone lithofacies (L10) is observed in Rio Bravo No. 2 and cores located in the north part of the study area (Kuhlman No. 3-A, Schoenhal No. 1, and Sam Hill No. 2-A). L10 is interpreted to have formed by carbonate sediment being transported from the shelf and proximal slope into deeper water by gravity-flow processes. Evidence of transport is the mixture of biota having been produced in different environments (e.g., crinoids, trilobites, and tabulate corals). The transport mechanism is not fully understood because of the density differences between carbonates and siliciclastic sediments. This lithofacies is possibly deposited by turbidity currents (in Kuhlman No. 3-A, Schoenhal No. 1, and Sam Hill No. 2-A, continuous lateral extension on wireline log correlation) or sliding (in Rio Bravo No. 2, no lateral extension between wells within 1.5 miles) (Prothero and Schwab, 2004).

Fine-grained sediments (clay-size and very fine silt-size particles) could have been transported into the basin by gravitational settling, flocculation and pelletization (Potter et al., 2005). Laminated calcareous to siliceous mudstone lithofacies is interpreted to occur in the basin below storm-wave base. The preservation of laminae indicates the lack of burrowing organisms and suggests deposition in a lower oxygenated setting. This lithofacies is interpreted to be deposited by low-density turbidity currents (Te division of Bouma, 1962) and possibly reworked by bottom current. Thin shells of organisms (e.g., brachiopods and ostracods) are considered to be transported from shallower water (outer shelf or upper slope) by turbidity currents. Laminae were formed by processes that sorts silt form mud (Stow and Bowen, 1978, 1980; McCave and Jones, 1988). The concentrated skeletal fragment layers at the base of this lithofacies are interpreted as transported skeletal debris (Loucks and Ruppel, 2007). Very thin to thin-laminated argillaceous mudstone was deposited by settling from dilute turbidity currents and reworking by bottom currents. This lithofacies contains a large terrigenous component as suggested by low values of Si/Ti and Si/Al ratio. The terrigenous components might be sourced by the outward diffusion of fluvial-deltaic discharge, low-density turbidity currents down channels or resuspension by bottom currents (Stow and Piper, 1984). The massive to faintly laminated mudstone is interpreted to be related to hemipelagic suspension settling as discussed by Stow and Piper (1984) and/or by diluted turbidity currents as described by Stanley (1981). The indistinctive laminations are related to the lack of coarser silt and very fine sand (Piper and Stow, 1984), compaction of dark colored organic-rich peloids, and/or small grain size variation. Accumulation rate of massive mud strata by hemipelagic settling is generally less than the accumulation rate by settling from detached low-density turbidity currents (Stanley, 1981). If the sedimentation rate of the sediment is too high, the organic material will be diluted.

If the sedimentation rate was too slow, the organic material probably could not have accumulated fast enough to outpace bacterial degradation (Loucks and Ruppel, 2007).

DEPOSITIONAL SETTING

The depositional setting of the Cherokee mudstones was below storm-wave base under anoxic to dysoxic condition as evidenced by the general lack of bioturbation (Loucks and Ruppel, 2007), precipitation of pyrite (Loucks and Ruppel, 2007), and enriched redox-sensitive trace elements (e.g., Mo, Zn, V, Cu, Ni) (Algeo and Maynard, 2004).

High TOC in mudstones is related to anoxic depositional conditions, high organic matter productivity, and slow sedimentation rate (Potter et al., 2004). Depositional environmental conditions of the laminated mudstone was suboxic to dysoxic as evidenced by the generally low Mo concentration and enriched suboxic proxies (Zn, V, Cu, Ni) as noted by Calvert and Pedersen (2007). The laminated mudstone shows a wide range of TOC (0.55% to 3.32 wt%). The low TOC may be the result of 1) dilution of organic matter by high volume of sediment influx, and/or 2) pauses of oxygen-rich waters may have been brought into the deepwater anoxic setting by turbidity current events. Concentration of Mo, Zn, V, Cu, and Ni is depleted in thin-laminated argillaceous mudstone lithofacies (L7), indicating suboxic conditions (Algeo and Maynard, 2004). L7 has poor TOC (less than 1.5 wt%), which corresponds to the low concentration of Mo, Zn, V, Cu, Ni. With the significant high clay-mineral content (Table 2) and enriched Ti concentration, the low TOC may result from the dilution of organic matter by high volumes of terrigenous sediment influx. Mo, Zn, V, Cn, and, Ni are significantly enriched in massive to faintly laminated mudstone lithofacies (L8). Total organic carbon of L8 at 9681.1 ft is 6.77wt%. L8 is interpreted to be deposited in anoxic bottom-water conditions. Although faunal fossils are common in the Cherokee group, they were interpreted to be dominantly transported from

adjacent shelves and upper-slope settings. The transported biota that may have lived in these severe bottom-water conditions for a short time are termed doomed pioneers (Follmi and Grimm, 1990). As discussed above, the sediment gravity-flow is a short-lived, relatively high-energy event deposit. It is possible that the oxygen associated with the current could have allowed for a bloom of short-lived agglutinated foraminifera.

CONTROLS ON DEPOSITIONAL CYCLES

Pennsylvanian stratal architecture in midcontinent is most commonly interpreted to be dominated by high-frequency, high-amplitude glacioeustatic fluctuations resulting from the waning and waxing of Gondwanan ice sheets (Veevers and Powell, 1987; Heckel, 1994). Klein (1994) attempted to quantify the influence of tectonic subsidence, short-term glacial eustasy, and long-term climate change on Pennsylvanian cyclic deposition in the midcontinent area, and concluded that Desmoinesian sea-level changes were influenced strongly by tectonic subsidence, especially in the basin area. The estimated sea-level changes in Pennsylvanian cycles are ~50-150 m (Moore 1958, 1964; Heckel 1977; Gerhard, 1991; Algeo and Heckel, 2008). Water depth in the deep basin was estimated as several hundred meters and varied through time in response to episodes of basin subsidence and fill (Algeo and Heckel, 2008). Heckel (2008) concluded that at least three transgression-regression cycles occurred on the shelf (marked by Verdigris Limestone, Tiawah Limestone, and Inola Limestone) and were related to short-term waxing and waning of ice sheets on Gondwana. In the study area, only the shale marker bed that capped the Verdigris Limestone was found (FS3).

A major change of the orientation and shape of sand-body geometries was observed between Package 3 (bounded by FS2 and FS3) and Package 4 (bounded by FS3 and FS4) (discussed in regional stratigraphic framework section) (Figure 15C, 15D). The deposition

of coarse-grained sediments may be controlled by the accommodation created by syndepositional subsidence of the basin and constant sediment supply from the Wichita-Amarillo Mountain uplift from south. The sandstone thickness in package 4 is significantly reduced, and may be related to the shut-down of sediment supply from the Wichita-Amarillo Mountain uplift, change on basin subsidence and fill (Algeo and Heckel, 2008), and/or glacial eustasy (Heckel, 2008). Autogenic processes, such as lobe switching and channel avulsion and migration (Muto and Steel, 2004; Van Dijk et al., 2009; Hubbard et al., 2009) can also produce a cyclic stratigraphic record. Given the magnitude of depositional cycles (less than 2 m [6.6 ft]) suggested by Sweet and Soreghan (2012), the depositional cycles seen in Cherokee core are likely related to autogenic processes. Nevertheless, it is difficult to conclude which mechanism is dominant in producing and controlling depositional cycles without very precise temporal and geometric control.

RESERVOIR PROPERTIES

Porosity and permeability were measured on 47 core plugs by Weatherford Labs. The results show a wide range of porosity (0.5 to 14.9%) and a relativity narrow range of permeability (less than 0.001 to 0.389 md) (Figure 4; Appendix II). Mean porosity is 4.5% and mean permeability is 0.368 md. Overall, the Cherokee sandstones and mudstone are tight.

Figure 4B shows the reservoir quality by each lithofacies. The massive sandstone lithofacies and sandy siliciclastic conglomerate lithofacies in the Sam Hill No.1 well and Flower Thrust No. 3-8 well (Figure 4A) have the best reservoir quality with mean permeability 0.381 and 0.389 md, respectively (Figure 4A). Full reservoir-quality statistics are provided in Appendix II.

The massive sandstone lithofacies, planar laminated to ripple-cross laminated sandstone lithofacies and sandy matrix conglomerate lithofacies from channel-fills and proximal lobes deposits yield better reservoir quality than the lobe margin and channel-levee deposits (Figure 17). Marchand et al. (2015) documented the similar relationship between reservoir architectural elements and reservoir quality in Paleogene deep-water reservoirs in Gulf of Mexico. Sediments deposited by high-energy flows are common in the channels and proximal lobe areas and are coarser in grain-size. The high-energy flows transit to low-energy flows down slope or when flow spills over the banks and the system becomes unconfined, which generally occurs in the channel-levee and lobe margin and fringe areas.

Massive sandstone lithofacies (L4) and planar laminated to ripple cross-laminated sandstone lithofacies (L5) show better reservoir quality than carbonate lithofacies (L10 and L11) in general (Figure 4B). Grainstones and grain-dominated packstones have better porosity and permeability than peloidal mud-dominated packstones (Figure 4B).

The reservoir quality is also related to sediment sources. The massive sandstone (L4) and laminated sandstone lithofacies (L5) show better reservoir quality in wells from the northern part of the study area (Kuhlman No. 3-A, Schoenhal No. 1, and Sam Hill No. 2-A) than wells from the south part of the study area (Flower Thrust No. 3 and Marjorie Campbell No. 1) (Figure 4A). Coarse-grained sediments (L1, L2, L3, L4, L5, and L6) in the Flower Thrust No. 3 and Marjorie Campbell No. 1 wells are rich in ductile grains (mud-clasts, micas, metamorphic and volcanic rock fragments, and organic particles) and poorly-sorted. Reservoir quality is influence by the abundance of ductile grains because they promote compactional porosity loss as suggested by Marchand et al. (2015). The muddy matrix conglomerate sandstone lithofacies that was deposited by cohesive-debris flows is only observed in these two wells. The very fine-silt to clay-size matrix has the ability to

block pore throats and decrease permeability. The reservoir quality of wells in the northern part of study area (Kuhlman No. 3-A, Schoenhal No. 1, and Sam Hill No. 2-A) is mainly controlled by degree of cementation. The more cemented sandstones show much lower porosity than the poorly-cemented sandstones.

The interparticle pores, intraparticle pores, and organic-matter nanopores reported in mudrocks by Loucks et al. (2012) are observed in the laminated mudstone (Figure 17). The totally porosity of the laminated mudstone sample is less than 1% by visual estimation. Intraparticle pores are the dominant pore type in the mudstone sample analyzed. The intraparticle pores include: 1) moldic pores formed by dissolution (e.g., calcite and dolomite), 2) intragrain pores within peloids and phosphate, 3) intercrystalline pores within pyrite framboids, and 4) pores along the cleavage planes of clay particles (see Loucks et.al, 2012 for discussion of these pore types). Interparticle pores are observed around the rim of rigid minerals. Organic-matter pores are observed but are rare in the sample (Figure 18). Most of the organic particles do not contain organic-matter pores. The effective porosity in the mudstone is poor because of the lack of interparticle pores and organic-matter pores (Loucks et al., 2012). More samples need to analyze to actually evaluate reservoir quality in the mudstone.

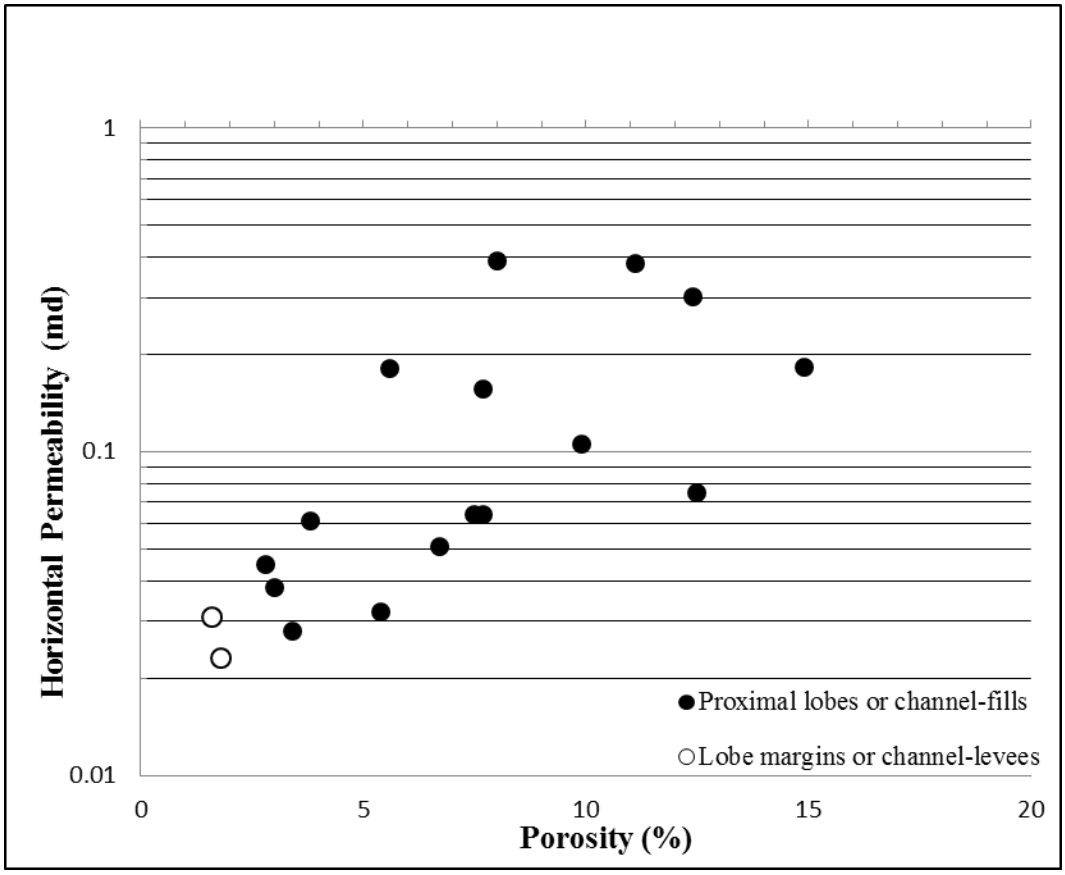

Figure 17. Porosity-permeability relationships in the proximal lobes or channel-fill deposits and lobe margin or channel-levee deposits.

TOTAL ORGANIC CONTENT

Total organic carbon (TOC) in the mudstones in the Cherokee unit ranges from 0.6 to 6.8 wt%. The massive to faintly laminated siliceous mudstone lithofacies (L8) has the highest mean TOC value (3.7 wt%) of the three mudstone types (Table 3). The laminated mudstone lithofacies (L6) displays a wide distribution of TOC ranging from 0.6% to 3.3 wt%. The very thin to thin-laminated argillaceous mudstone lithofacies (L7) is organic good (mean TOC is 1.2 wt%). Calculated vitrinite reflectance (R_o) shows that all mudstone samples are in the oil window (Figure 5B). A Dembicki plot (Dembicki, 2009) was created to examine the potential of hydrocarbon generation (Figure 5A). This plot considered TOC,

S2 (generated hydrocarbon in the pyrolysis experiment) and S1+S2 (pre-existing and generated hydrocarbons) to evaluate mudstone hydrocarbon generation potential. The plot displays that hydrocarbon generation potential ranges from fair to excellent. The samples with excellent hydrocarbon generation potential are all from the massive to faintly laminated siliceous mudstone lithofacies. Kerogen types are Type II and Type III kerogen inferred from Pseudo Van Krevelen plot and plots of hydrogen index versus Tmax provided by GeoMark Research. Presence of organic particles with and without organic-matter pores also supported this interpretation of mixed organic types (Figure 18) (Loucks et al., 2012).

Table 3. Total Organic Carbon Content in Mudstone Lithofacies.

	Laminated calcareous to siliceous mudstone	Very thin to thin-laminated argillaceous mudstone	Massive to faintly laminated siliceous mudstone
Mean TOC (wt %)	1.41	1.22	3.74
Minimum TOC (wt %)	0.55	1.01	2.01
Maximum TOC (wt %)	3.32	1.42	6.77

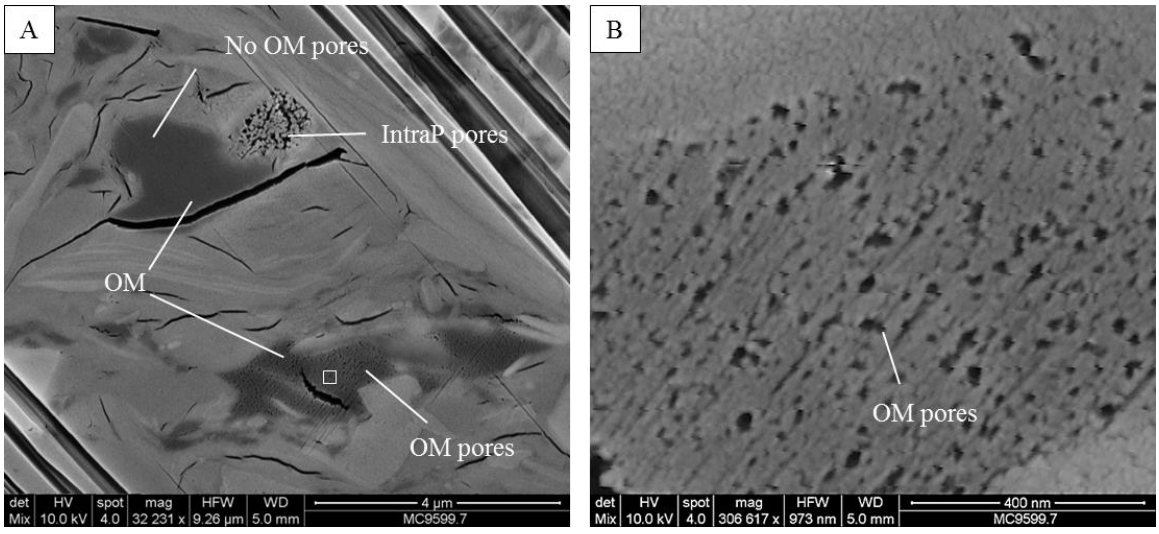

Figure 18

Figure 18. Pore types in laminated siliceous mudstone: Marjorie Campbell No. 1, 9599.7 ft (2926 m). TOC is 2.18 wt%, Calculated Ro is 0.8%. Organic matter pores are present but rare in this sample.

CONCLUSIONS

A subsurface data set, consisting of 1980 wireline-logs and six cores, permits characterization of the Cherokee Group in the northwest part of the Anadarko Basin. The Cherokee Group in Texas Panhandle is composed of mudstones interbedded with siliciclastic and carbonate strata in a deep-water basinal system. The Wichita-Amarillo Mountain uplift to the south and Kansas Shelf to the north are the two major sediment sources. The deposition of the Cherokee Group in the study area was under dysoxic to anoxic bottom conditions developed below storm-wave base and below the oxygen-minimum zone. Sedimentation was dominated by gravity flows and suspension settling and reworking by bottom currents. Skeletal allochems were transported into the basin from the shallower outer shelf and upper slope.

Eleven lithofacies were identified from the six cores in the Cherokee Group in Texas Panhandle. Two depositional patterns, proximal lobe/amalgamated channel and distal lobe/ channel-levee were interpreted from the lithofacies associations and gross-sandstone isopachous maps.

Depositional cycles are interpreted to have been predominately driven by autogenic processes such as channel avulsion and migration and lobe shifting. Glacial eustasy influenced the cyclic deposition of the Cherokee Group in the basin as it did in the Pennsylvanian elsewhere, but local tectonics may have also been an important control for cycle development.

Reservoir qualities of coarse-grained sediments are related to controlled by grain types (e.g., abundance of ductile grains), grain texture (grain size and sorting), and degree of cementation. Sandy matrix conglomerate lithofacies, massive lithofacies, planar laminated to ripple cross-laminated sandstone lithofacies, and muddy matrix conglomerate

sandstone lithofacies show better reservoir quality than carbonate lithofacies in general. The amalgamated channel-fill/proximal lobe deposits show better reservoir quality that the channel-levee/lobe margin deposits. The analyzed mudstone sample show poor effective porosity, but more samples need to be analyzed to actually evaluate reservoir quality in the mudstone. Mudstones in Cherokee Group are all in oil generation window. Massive to faintly laminated mudstone lithofacies that was deposited by hemipelagic settling has high TOC and show good to excellent hydrocarbon generation potential.

This study contributes a deep-water slope to basin-floor depositional model that was previously unexplored and defines sediment sources and depositional setting and cycles of the Cherokee Group in the Anadarko Basin, Texas Panhandle. The response of the depositional system to autogenic processes resulted in predictable lithofacies distribution and stratigraphic stacking pattern that helps with the characterization of the hybrid mudstone system.

Appendix

Table 4. Mineralogical Analysis of the Cherokee Group Based on XRD Data

	Laminated calcareous to siliceous mudstone			Very thin to thin-laminated argillaceous mudstone			Massive to faintly laminated siliceous mudstone			Peloidal packstone			Grainstone and grain-dominated packstone		
	avg	min	max	avg	min	max	avg	min	max	avg	min	max	avg	min	max
Quartz	9.93	0.83	15.55	9.08	8.83	9.40	9.82	5.13	12.83	5.33	5.33	5.33	2.08	2.08	6.00
K-Feldspar	1.31	0.16	4.07	1.16	0.70	1.92	0.98	0.47	1.37	0.46	0.46	0.46	0.26	0.26	2.15
Plagioclase	3.33	0.27	12.05	2.50	2.40	2.66	3.40	1.06	5.74	1.63	1.63	1.63	1.09	1.09	5.10
Fe-Calcite	0.00	0.00	0.00	0.00	0.00	0.00	1.88	0.00	7.53	0.00	0.00	0.00	3.62	3.62	7.25
Calcite	6.38	0.15	19.37	1.16	0.00	2.58	5.13	0.81	9.08	3.42	3.42	3.42	20.62	20.62	36.31
Aragonite	1.26	0.00	2.14	0.00	0.00	0.00	0.00	0.00	0.00	0.00	0.00	0.00	2.40	2.40	21.59
Fe-Dolomite	5.09	0.59	22.41	0.16	0.00	0.48	2.16	0.00	6.69	18.30	18.30	18.30	3.49	3.49	19.83
Dolomite	0.00	0.00	0.00	0.00	0.00	0.00	1.06	0.00	3.37	0.00	0.00	0.00	6.26	6.26	30.70
Siderite	0.08	0.00	0.45	0.82	0.00	2.47	0.18	0.00	0.88	0.00	0.00	0.00	0.02	0.02	0.15
Pyrite	0.28	0.06	1.02	0.85	0.00	1.47	0.71	0.22	1.39	0.48	0.48	0.48	0.04	0.04	0.16
Apatite	0.22	0.00	0.57	0.00	0.00	0.00	0.00	0.00	0.00	0.00	0.00	0.00	0.13	0.13	0.63
Gypsum	0.11	0.00	0.91	0.45	0.00	0.91	0.17	0.00	0.52	2.90	2.90	2.90	0.08	0.08	0.56
Natrojarosite	0.00	0.00	0.00	1.69	0.00	3.38	0.17	0.00	0.69	2.36	2.36	2.36	0.75	0.75	1.46
Illite&Mica	3.86	0.60	11.39	9.41	8.16	10.45	4.62	2.06	5.69	0.23	0.23	0.23	0.03	0.03	0.19
Kaolinite	0.65	0.15	1.15	0.95	0.38	1.62	0.66	0.35	1.00	0.51	0.51	0.51	0.06	0.06	0.45
Chlorite	1.42	0.14	3.86	1.93	0.72	2.86	1.10	0.62	1.41	3.10	3.10	3.10	0.84	0.84	1.76

Table 4 (continued)

Clay minerals	5.93	0.89	14.04	12.29	10.73	14.93	6.38	3.10	8.00	7.43	7.43	7.43	3.43	3.43	13.25
Silicicalstic	14.56	1.25	26.46	12.74	12.31	13.14	14.20	6.67	19.43	21.72	21.72	21.72	32.64	32.64	36.31
Carbonate	11.93	1.60	33.41	1.32	0.00	2.58	9.60	2.43	23.29	35.63	35.63	35.63	37.14	37.14	44.48

	Grainstone and grain-dominated packstone			Massive sandstone			Muddy matrix conglomerate		
	avg	min	max	avg	min	max	avg	min	max
Quartz	2.08	6.00	18.23	10.40	6.49	13.92	9.47	3.32	11.77
K-Feldspar	0.26	0.20	3.17	3.95	0.20	5.95	3.05	0.20	7.05
Plagioclase	1.09	3.04	15.40	12.50	8.44	14.71	10.71	0.46	14.75
Fe-Calcite	3.62	0.00	7.25	0.00	0.00	0.00	1.75	0.00	5.24
Calcite	20.62	0.00	22.73	1.73	0.00	5.90	2.74	0.00	15.35
Aragonite	2.40	0.00	21.59	0.00	0.00	0.00	0.00	0.00	0.00
Fe-Dolomite	3.49	0.00	2.72	4.39	0.90	8.86	2.99	0.00	14.55
Dolomite	6.26	0.00	1.44	0.00	0.00	0.00	1.18	0.00	2.32
Siderite	0.02	0.00	0.40	0.00	0.00	0.00	0.00	0.00	0.00
Pyrite	0.04	0.04	0.56	0.11	0.04	0.26	0.26	0.08	0.54
Apatite	0.13	0.31	1.83	0.00	0.00	0.00	0.00	0.00	0.00
Gypsum	0.08	0.00	0.00	0.00	0.00	0.00	0.00	0.00	0.00
Natrojarosite	0.75	0.00	0.00	0.00	0.00	0.00	0.00	0.00	0.00

Table 4 (continued)

Illite&Mica	0.03	0.45	3.86	1.21	0.75	1.87	1.67	0.79	2.32
Kaolinite	0.06	0.00	0.81	0.42	0.19	1.00	1.04	0.31	1.76
Chlorite	0.84	0.00	1.76	1.89	0.97	5.21	2.24	0.10	4.52
Clay minerals	3.43	0.45	4.91	3.52	2.36	7.52	5.21	1.20	7.45
Silicicalstic	32.64	11.67	29.53	26.84	18.18	33.14	23.23	3.97	30.99
Carbonate	37.14	3.78	29.14	6.12	0.90	13.62	7.19	0.86	29.90

Table 5. Porosity and Permeability of Reservoir Architecture Element

Proximal Lobes or channel-fills				
Well name	Depth (ft)	Lithofacies	Porosity (%)	Permeability (md)
Flowers Trusts No. 3-8	9849.0	L4	5.6	0.181
Flowers Trusts No. 3-8	9856.1	L4	7.7	0.064
Flowers Trusts No. 3-8	9866.7	L4	3.8	0.061
Flowers Trusts No. 3-8	9889.8	L4	7.7	0.156
Flowers Trusts No. 3-8	9895.8	L4	7.5	0.064
Flowers Trusts No. 3-8	9902.0	L4	9.9	0.106
Flowers Trusts No. 3-8	9923.1	L4	3.4	0.028
Flowers Trusts No. 3-8	9891.2	L3	8.0	0.389
Kuhlman No. 3-A	7979.5	L4	12.4	0.301
Kuhlman No. 3-A	7984.5	L4	12.5	0.075
Kuhlman No. 3-A	7997.0	L4	5.4	0.032
Kuhlman No. 3-A	7990.0	L5	14.9	0.182
Kuhlman No. 3-A	8002.5	L5	25.1	7.717

Table 5 (continued)

Kuhlman No. 3-A	8022.5	L5	1.3	<.001
Sam Hill No. 2-A	7155.0	L5	2.8	0.045
Sam Hill No. 2-A	7223.0	L5	6.7	0.051
Sam Hill No. 2-A	7215.0	L4	1.4	<.001
Sam Hill No. 2-A	7227.0	L4	11.1	0.381
Sam Hill No. 2-A	7233.0	L4	3.0	0.038
Lobe margins or channel-levees				
Well name	Depth (ft)	Lithofacies	Porosity (%)	Permeability (md)
Marjorie Campbell No. 1	9563.2	L4	1.6	0.031
Marjorie Campbell No. 1	9635.5	L4	1.5	<.001
Marjorie Campbell No. 1	9656.5	L4	5.8	<.001
Marjorie Campbell No. 1	9718.5	L4	1.6	<.001
Marjorie Campbell No. 1	9580.5	L5	1.9	<.001
Marjorie Campbell No. 2	9653.7	L5	4.3	<.001
Sam Hill No. 2-A	7210.0	L5	1.1	<.001
Flowers Trusts No. 3-8	9920.2	L5	1.8	0.023

Appendix III. Core Descriptions

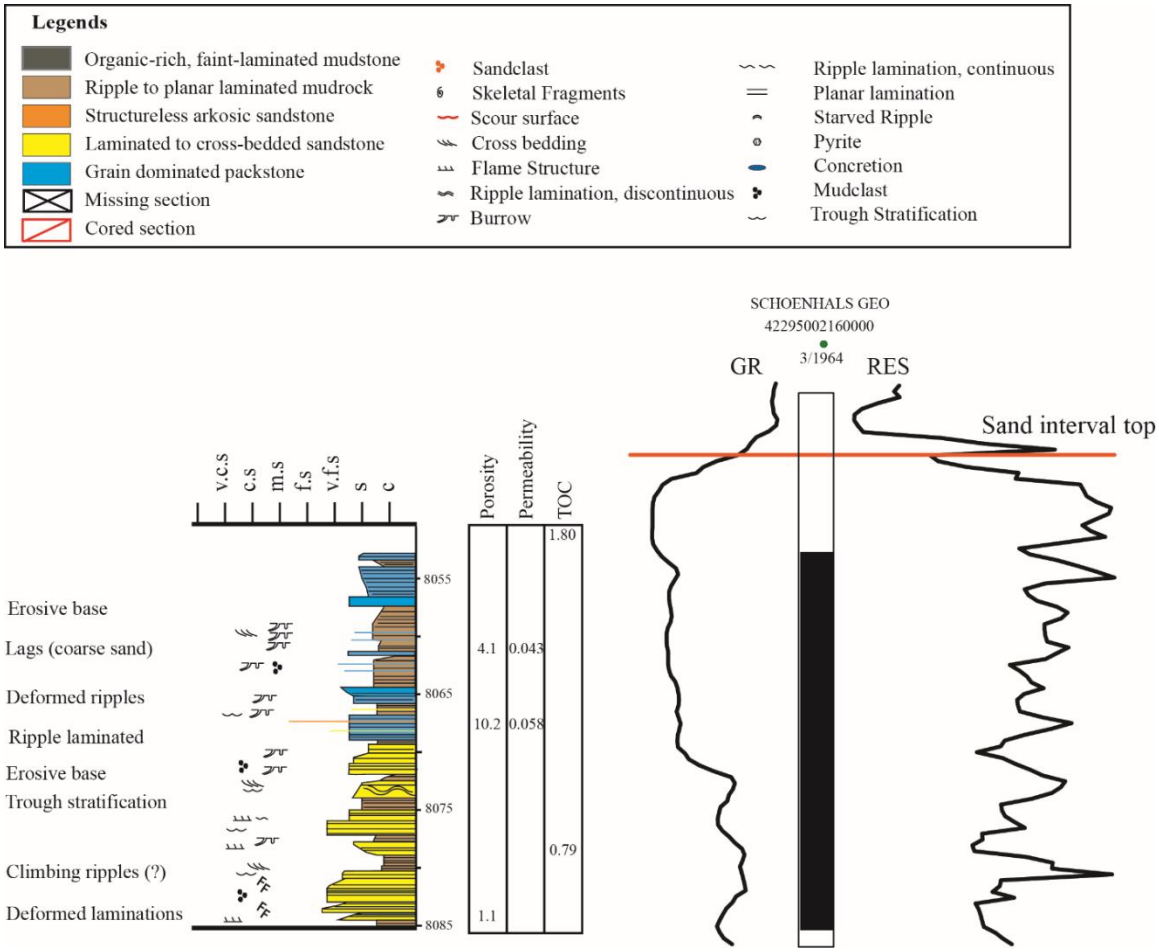

Schoenhal No. 1

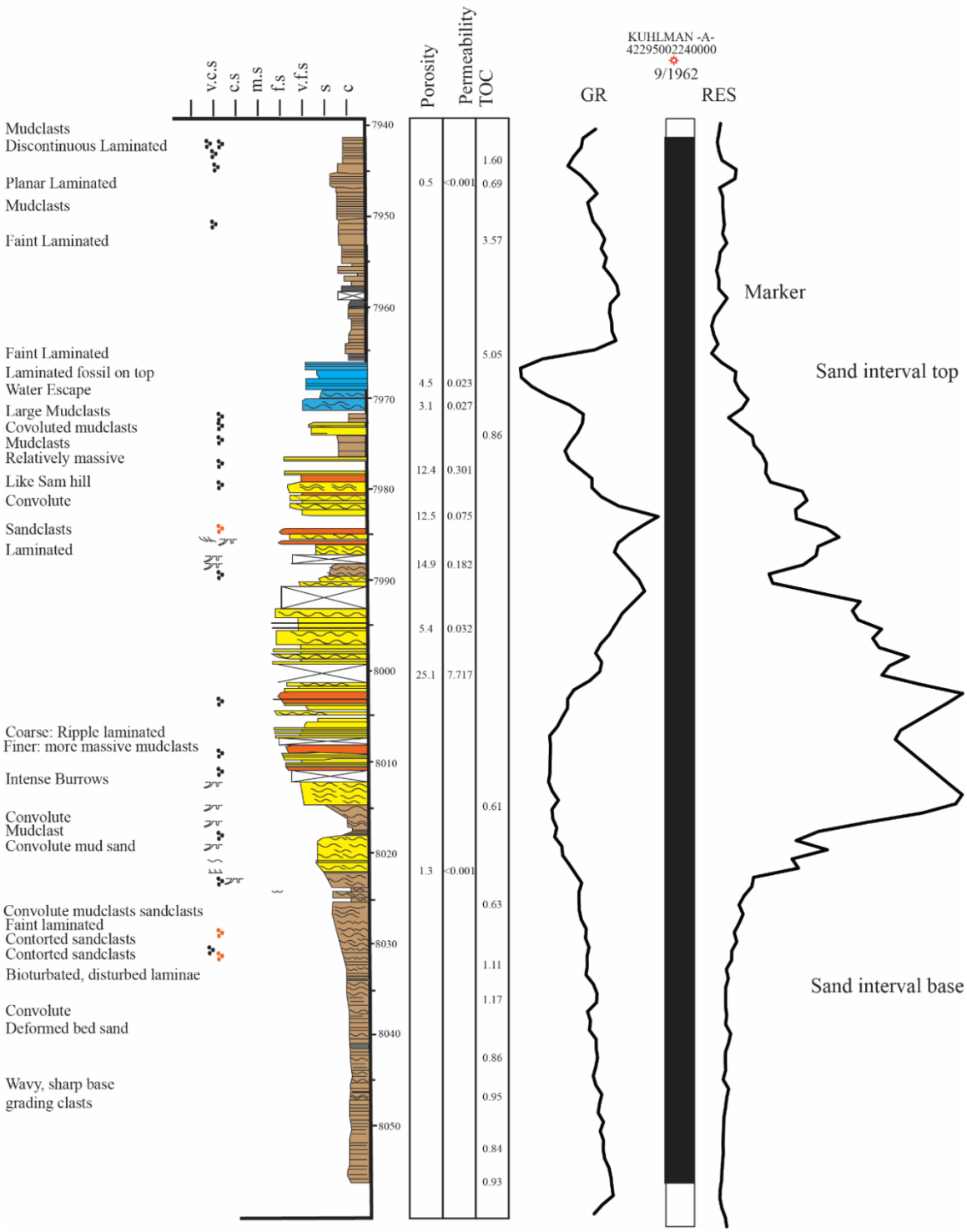

Kuhlman No. 3-A

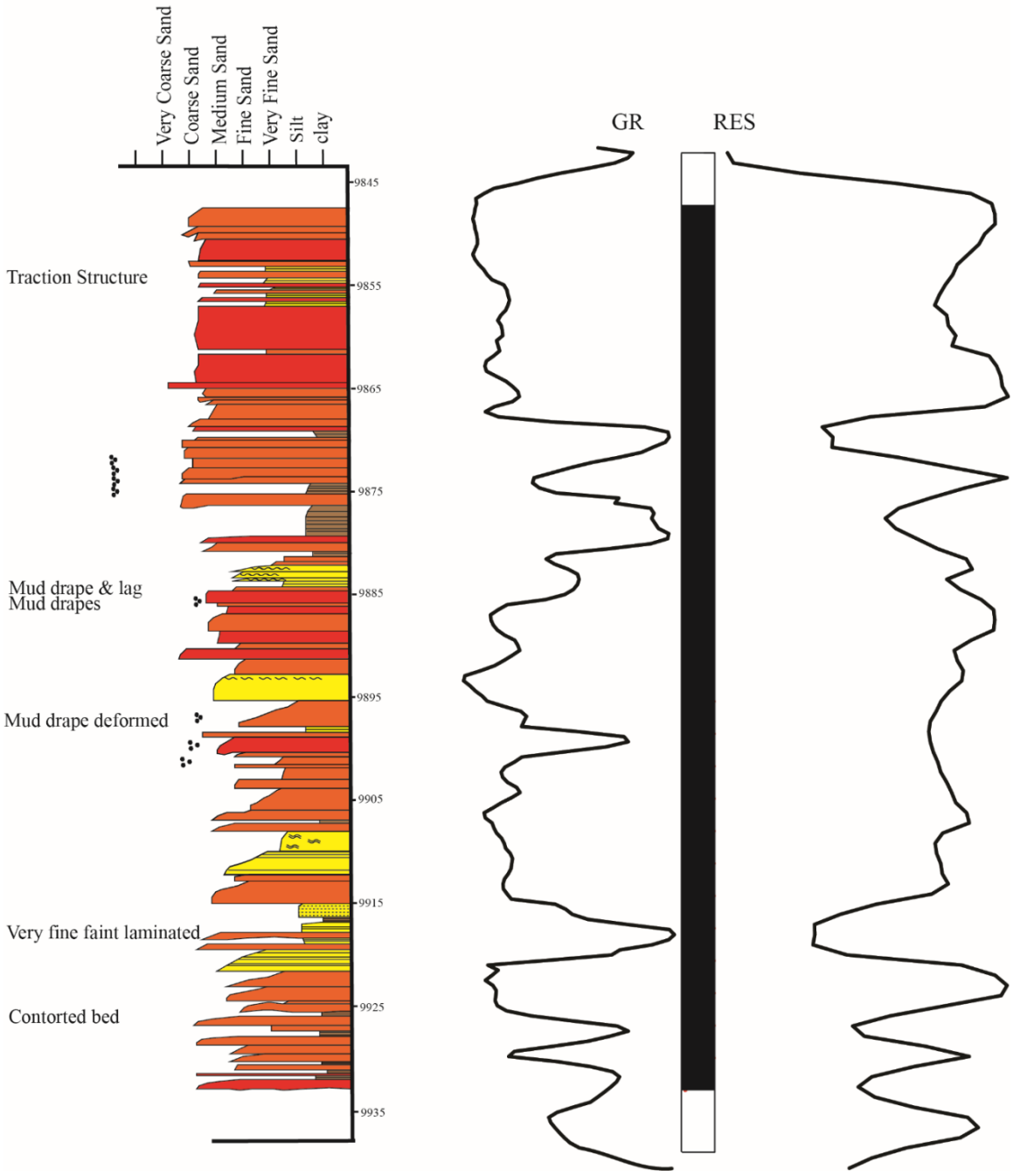

Flowers Trusts No. 3-A

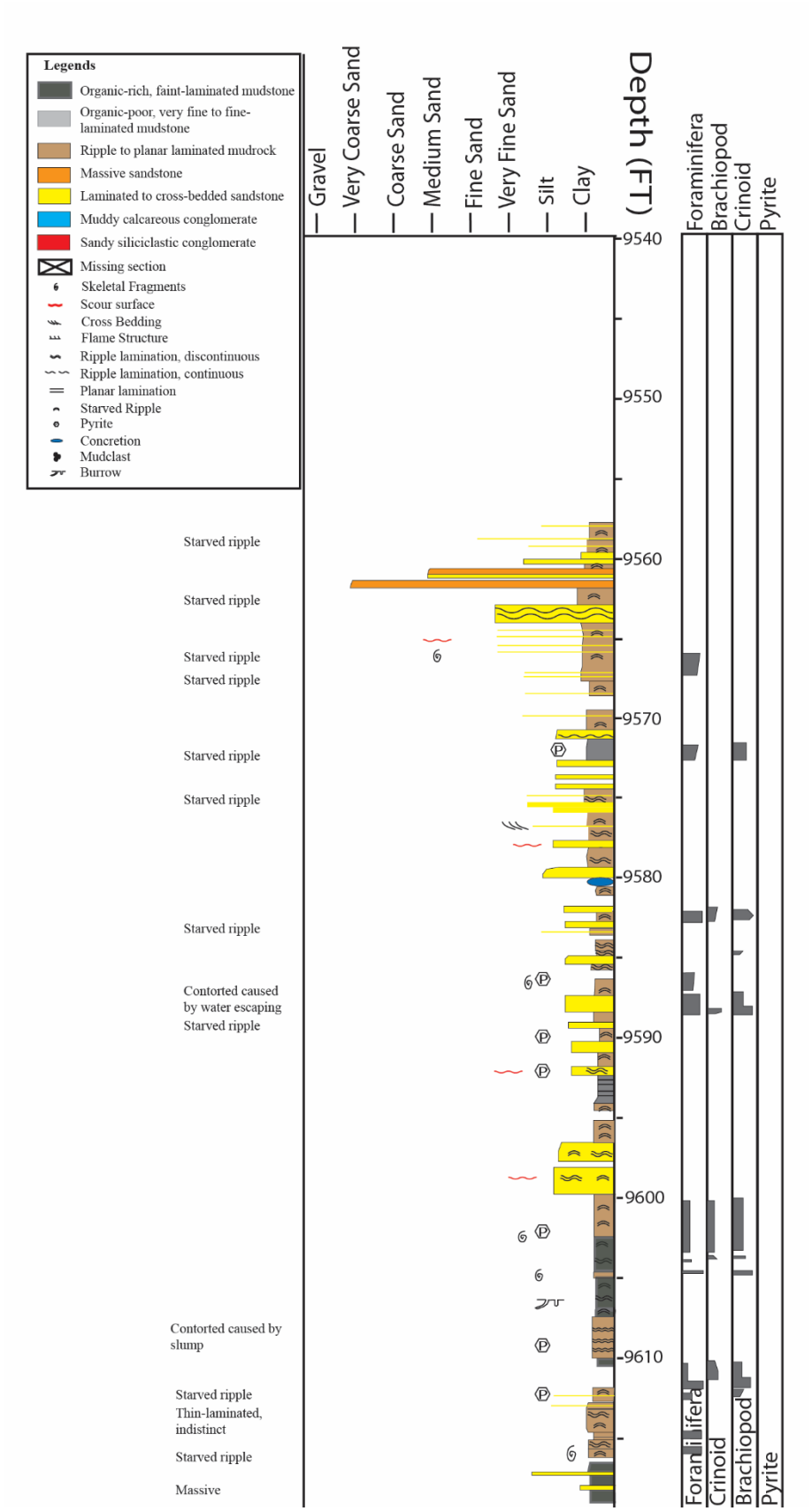
Legends
Organic-rich, faint-laminated mudstone
Organic-poor, very fine to fine-laminated mudstone
Ripple to planar laminated mudrock
Massive sandstone
Laminated to cross-bedded sandstone
Muddy calcareous conglomerate
Sandy siliciclastic conglomerate
Missing section
Skeletal Fragments
Scour surface
Cross Bedding
Flame Structure
Ripple lamination, discontinuous
Ripple lamination, continuous
Planar lamination
Starved Ripple
Pyrite
Concretion
Mudclast
Burrow
Gravel
Very Coarse Sand
Coarse Sand
Medium Sand
Fine Sand
Very Fine Sand
Silt
Clay
Depth (FT)
9540
9550
9560
9570
9580
9590
9600
9610
Foraminifera
Brachiopod
Crinoid
Pyrite
Starved ripple
Starved ripple
Starved ripple
Starved ripple
Starved ripple
Starved ripple
Starved ripple
Contorted caused by water escaping
Starved ripple
Contorted caused by slump
Starved ripple
Thin-laminated, indistinct
Starved ripple
Massive
Foraminifera
Crinoid
Brachiopod
Pyrite

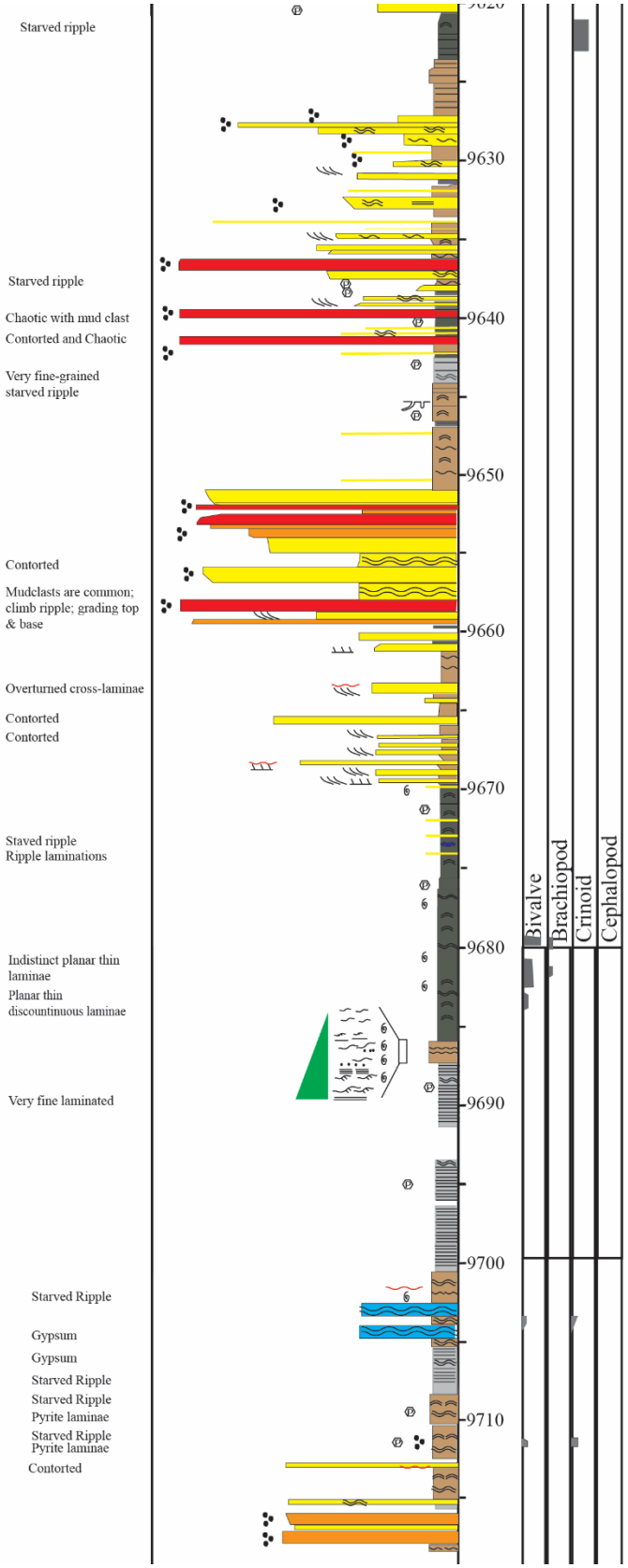
Starved ripple
Starved ripple
Chaotic with mud clast
Contorted and Chaotic
Very fine-grained starved ripple
Contorted
Mudclasts are common; climb ripple; grading top & base
Overturned cross-laminae
Contorted
Contorted
Staved ripple
Ripple laminations
Indistinct planar thin laminae
Planar thin discountinuous laminae
Very fine laminated
Starved Ripple
Gypsum
Gypsum
Starved Ripple
Starved Ripple
Pyrite laminae
Starved Ripple
Pyrite laminae
Contorted
9630
9640
9650
9660
9670
9680
9690
9700
9710
Bivalve
Brachiopod
Crinoid
Cephalopod

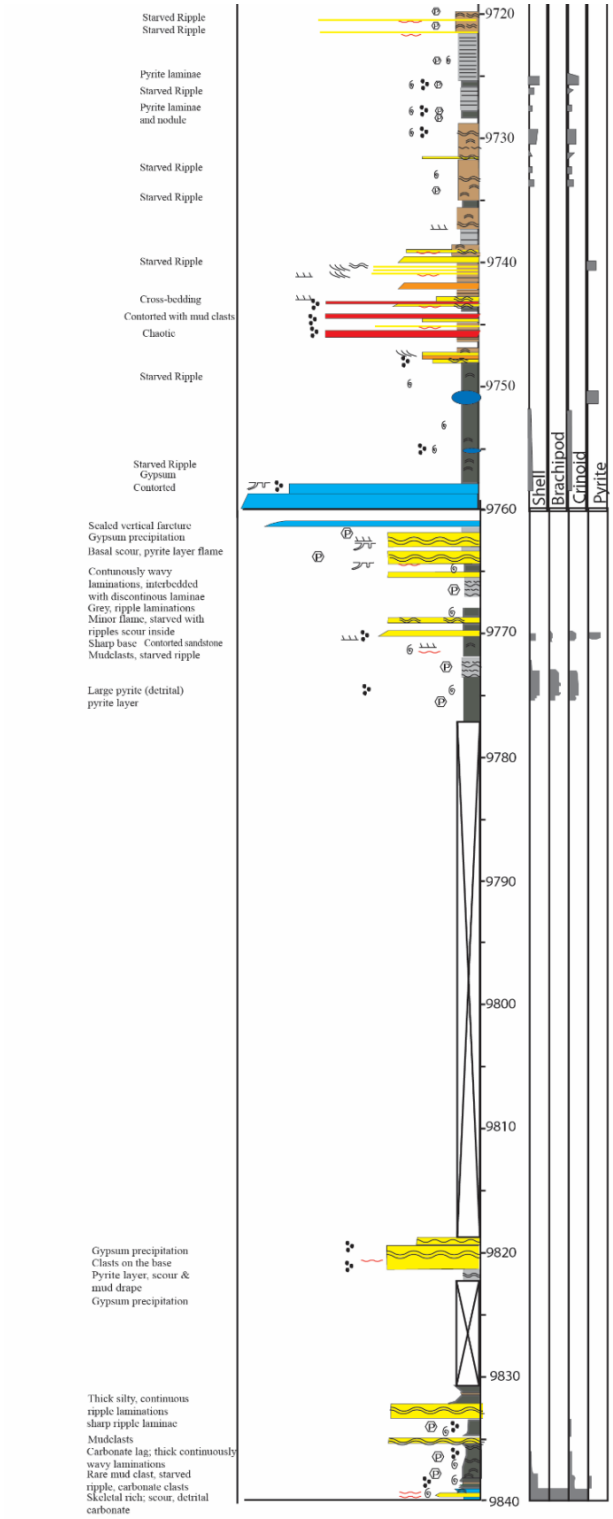

Marjorie Campbell No. 1

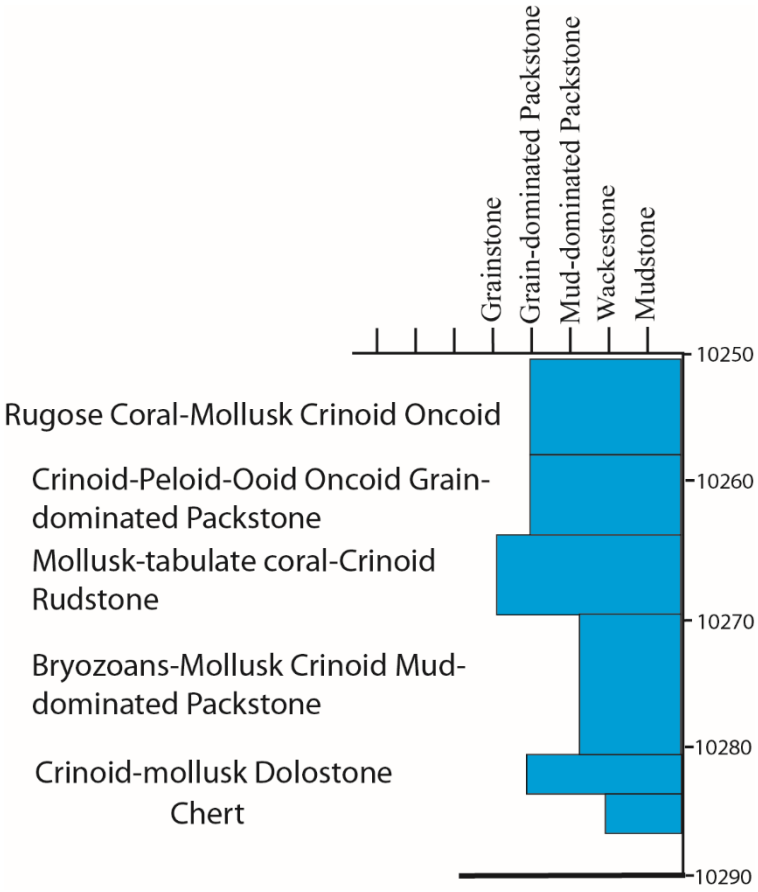

Rio Bravo No. 2

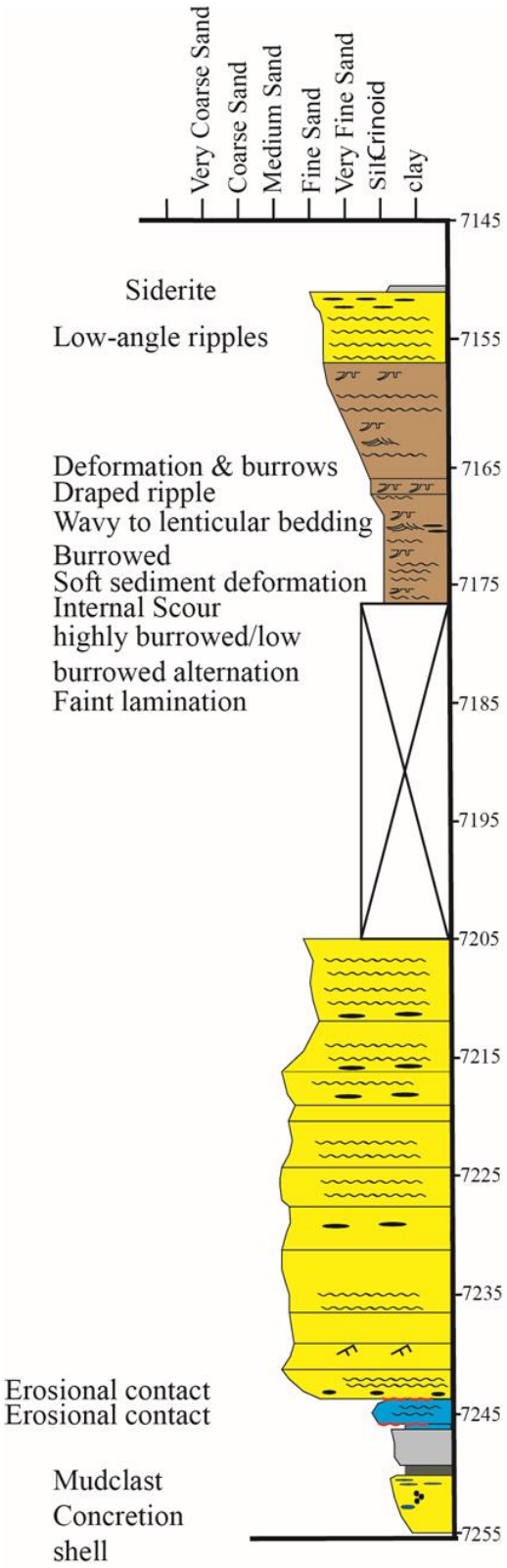

Sam Hill No. 2-A

References

Ambrose, W.A., and Hentz, T.F., 2011, Depositional systems and facies variability in tidally modified shelf and estuarine systems in the Pennsylvanian Cleveland Formation, Anadarko Basin, North Texas and western Oklahoma, in Ambrose, W. A., ed., Sequence stratigraphy, depositional systems, and hydrocarbon play analysis of the Pennsylvanian Cleveland Formation and Marmaton Group, Anadarko Basin, North Texas and western Oklahoma: The University of Texas at Austin, Bureau of Economic Geology, Report of Investigations No. 275, p. 35-66.

Anderson, C.J., Jr., 1992, Distribution of submarine fan facies of the upper Red Fork interval in the Anadarko basin, western Oklahoma: Oklahoma State University unpublished M.S. thesis, 275p.

Algeo, T.J., and Heckel, P.H., 2008, The Late Pennsylvanian midcontinent sea of North America: a review: Palaeogeography, Palaeoclimatology, Palaeoecology, 268, p. 205–221.

Algeo, T.J., and Maynard, J.B., 2004, Trace element behavior and redox facies in core shales of Upper Pennsylvanian Kansas-type cyclothems: Chemical Geology, v. 206, p. 289–318.

Al-Shaieb, Zuhair, Puckett, J.O., Abdalla, A.A., and Ely, P.B., 1994, Megacompartment complex in the Anadarko Basin: A completely sealed overpressured phenomenon, *in* Ortoleva, P.J., ed., Basin compartments and seals: American Association of Petroleum Geologists Memoir 61, p. 55–68.

Andrews, R. D., Campbell, J.A., and Northcutt, R.A., 1996, Fluvial-dominated deltaic (FDD) oil reservoirs in Oklahoma: The Skinner and Prue plays: Oklahoma Geological Survey Special Publication 96–2, 106 p.

Andrews, R.D., and Bottmann, R.D., 1997, Fluvial-dominated deltaic (FDD) oil reservoirs in Oklahoma: The Red Fork Play: Oklahoma Geological Survey Special Publication 97–1, 101 p.

Blakey, R.C., 2013, Paleogeography and tectonic history of North America: North American Key Time-Slice Paleogeographic Maps, Carboniferous Pennsylvanian (308 Ma) : <http://cpgeosystems.com/namkeyframe.html> Accessed March 7, 2016.

Boucher, Kurtis, 2009, Depositional setting, facies, and petroleum geology of the Cabaniss Group in portions of Washita, Custer, Blaine, Caddo, Canadian, and Grady

Counties, OK, Part 2: Shale Shaker, the Journal of the Oklahoma City Geological Society, May–June 2009, p. 223–238.

Bouma, A.H., 1962, Sedimentology of some Flysch Deposits: Amsterdam, Elsevier Publ. Co., 168 p.

Burruss, R.C., and Hatch, J.R., 1989, Geochemistry of oils and hydrocarbon source rocks, greater Anadarko Basin: Evidence for multiple sources of oils and long-distance oil migration, *in* Johnson, K.S., ed., Anadarko Basin symposium, 1988: Oklahoma Geological Survey Circular 90, p. 53–64.

Calvert, S.E., and Pedersen, T.F., 2007, Elemental proxies for palaeoclimatic and palaeoceanographic variability in marine sediments: interpretation and application, in Proxies in late Cenozoic paleoceanography, edited by C. Hillaire-Marcel and A. de Vernal: Elsevier, Oxford, p. 567-644.

Dembicki, H, Jr., 2009, Three common source rock evaluation errors made by geologists during prospect or play appraisals, AAPG Bulletin v. 93, No. 3, p. 341-356.

Dow, W.G., 1977, Kerogen studies and geological interpretations: Journal of geochemical exploration, v. 7, p. 79-99.

Evans, J.L., 1979, Major structura1 and stratigraphic features of the Anadarko Basin: in Pennsylvanian Sandstones of the Mid-Continent (Hyne, N.J., editor): Tulsa Geol. Soc. Spec. Pub., no. 1, p. 97-114.

FöIlmi, K.B., and K.A. Grimm, 1990, Doomed pioneers: Gravity-flow deposition and bioturbation in marine oxygen-deficient environments: Geology, v. 18, No.11, p. 1069-1072.

Gerhard, L.C., 1991, Stratigraphy in the modern generation: Lawrence, Kansas Geological Survey, Open File Report 91-24, 13 p.

Glass, J. L., 1981, Depositional environments, reservoir trends, and diagenesis of the Red Fork Sandstone in Grant and eastern Kay Counties, Oklahoma: Oklahoma State University unpublished M.S. thesis, 99 p.

Hansen, C.A., 1978, Subsurface Virgilian and Lower Permian Arkosic Facies, Wichita Uplift-Anadarko Basin, Oklahoma: Unpublished Master's Thesis, Oklahoma State University.

Hendrickson, W.J., P.W. Smith, and R.J. Woods, 2001, Regional correlation of Mountain-Front “washes” and relationship to marine sediments of Anadarko Basin and shelf,

in K.S. Johnson, ed., Pennsylvanian and Permian geology and petroleum in the southern Midcontinent, 1998 symposium: OGS Circular 104, p. 71-80.

Hickson, T.A. and Lowe, D.R., 2002, Facies architecture of a submarine fan channel-levee complex: the Juniper Ridge Conglomerate, Coalinga, California. Sedimentology, 49, p. 335-362.

Higley, D.K., compiler, 2014, Petroleum systems and assessment of undiscovered oil and gas in the Anadarko Basin Province, Colorado, Kansas, Oklahoma, and Texas—USGS Province 58: U.S. Geological Survey Digital Data Series DDS–69–EE, 327p., 8 pls.,*http://dx.doi.org/10.3133/ds69EE*.

Heckel, P.H., 1977, Origin of phosphatic black shale facies in Pennsylvanian cyclothems of Midcontinent North America: Bulletin of the American Association of Petroleum Geologists, v. 61, p. 1045-1068.

Heckel, P.H., 1991, Thin widespread Pennsylvanian black shales of Midcontinent North America: a record of a cyclic succession of widespread pycnoclines in a fluctuating epeiric sea. In: Tyson, R.V., Pearson, T.H. (Eds.), Modern and Ancient Continental Shelf Anoxia: Geol. Soc. London. Spec. Publ., vol. 58, p. 259–273.

Heckel, P.H., 1994, Evaluation of evidence for glacial-eustatic control over marine Pennsylvanian cyclothems in North America and consideration of possible tectonic effects. In: Dennison, J.M., Ettensohn, F.R. (Eds.), Tectonic and Eustatic Controls on Sedimentary Cycles. Concepts in Sedimentology and Paleontology, vol. 4: SEPM, p. 65–87.

Heckel, P.H., 2008, this volume, Pennsylvanian cyclothems in Midcontinent North America as far-fi eld effects of waxing and waning of Gondwana ice sheets, in Fielding, C.R., Frank, T.D., and Isbell, J.L., eds., Resolving the Late Paleozoic Ice Age in Time and Space: Geological Society of America Special Paper 44, p. 275-289.

Hentz, T.F., 2011, Chronostratigraphy and depositional history of the Pennsylvanian Marmaton Group and Cleveland Formation on a structurally complex shelf: western Anadarko Basin, Texas and Oklahoma, in Ambrose, W. A., ed., Sequence stratigraphy, depositional systems, and hydrocarbon play analysis of the Pennsylvanian Cleveland Formation and Marmaton Group, Anadarko Basin, North Texas and western Oklahoma: The University of Texas at Austin, Bureau of Economic Geology, Report of Investigations No. 275, p. 1-34.

Hubbard, S.M., de Ruig, M.J., and Graham, S.M., 2009, Confined channel-levee complex development in an elongate depocenter: Deep-water Tertiary strata of the Austrian Molasse Basin: Marine and Petroleum Geology, v. 26,

Johnson, C.L., 1984, Depositional environments, reservoir trends, and diagenesis of the Red Fork sandstones in portions of Blaine, Caddo, and Custer Counties, Oklahoma: Oklahoma State University unpublished M.S. thesis, 122 p.

Johnson, K.S., 1989, Geologic evolution of the Anadarko Basin: *in* K. S. Johnson, ed., Proceedings of the Anadarko Basin symposium: OCGS Circular 90, p. 3-12.

Johnson, K.S.; Amsden, T. W.; Denison, R. E.; Dutton, S. P.; Goldstein, A. G.; Rascoe, Bailey, Jr.; Sutherland, P. K.; and Thompson, D. M., 1988, Southern Midcontinent region, in Sloss, L. L. (ed.), Sedimentary cover-North American craton: Geological Society of America, The Geology of North America, v. D-2, p. 307-359.

Kane, I.A., and Pontén, A.S.M., 2012, Submarine transitional flow deposits in the Paleogene Gulf of Mexico: Geology, v. 40, p. 1119–1122.

Klein, G.D., 1994, Depth Determination and Quantitative Distinction of the Influence of Tectonic Subsidence and Climate on Changing Sea Level during Deposition of Midcontinent Pennsylvanian Cyclothems: Tectonic and Eustatic Controls on Sedimentary Cycles, v. 1, No. 1, p. 35-50.

Lambert, 2006, Interpretation of yhe Upper Red Fork Valley in the Anadarko Basin: A Comparison Study Between Processed, Reprocessed, and High Frequency Seismic Data: unpublished Masters thesis, Okla. State University, 44 p.

Lowe, D.R., 1982, Sediment gravity flows II: Depositional models with special reference to high density turbidity currents: J. Sed. Petrol., 52, p. 279–298.

Lowe, D.R., 1975, Water escape structures in coarse grained sediments: Sedimentology, v. 22, p. 157-204.

Loucks, R.G., and S.C. Ruppel, 2007, Mississippian Barnett Shale: Lithofacies and depositional setting of a deep-water shale-gas succession in the Fort Worth Basin, Texas, AAPG Bulletin v. 91, No. 4, p. 579-601.

Loucks, R.G., Reed, R.M., Ruppel, R.M., and Hammes, U., 2012, Spectrum of pore types and networks in mudrocks and a descriptive classification for matrix-related mudrock pores, AAPG Bulletin, v. 96, No. 6, p. 1071-1098.

Manley, P.L., Pirmez, C., Busch, W., and Cramp, A., 1997, Grain-size characterization of Amazon Fan deposits and comparison to seismic facies units, in Flood, R.D., Piper, D.J.W., Klaus, A., and Peterson, L.C., eds., Proceedings of the Ocean Drilling Program, Scientific Results, v. 155, p. 35-52.

Marchand, A. M., Apps, G., Li, W., & Rotzien, J. R., 2015, Depositional processes and impact on reservoir quality in deepwater Paleogene reservoirs, US Gulf of Mexico: AAPG Bulletin, 99(9), p. 1635-1648.

Masalimova, L., 2013, Stratigraphic architecture and flow dynamics of deep-water turbidite deposits: the Miocene lower Mount Messenger Formation in the Taranaki Basin in New Zealand, and the Oligocene Puchkirchen Formation in the Molasse Basin in Austria: unpublished doctoral thesis, Standford University, 211 p.

McCave, I.N., Jones, K.P.N. 1988, Deposition of ungraded muds from high-density non-turbulent turbidity currents: Nature 333, 250-52.

Middleton, G. V., and Hampton, M. A., 1973, Sediment gravity flows: mechanisms of flow and deposition: In: Turbidites and Deep-Water Sedimentation, pp. 1–38. SEPM Pacific Section, Short course lecture notes.

Mitchell, J., 2011, Horizontal drilling of deep granite wash reservoirs, Anadarko Basin, Oklahoma and Texas: Oklahoma City Geological Society Shale Shaker, September-Oklahoma, 2011, p. 118-167.

Moore, R. C., 1958, Historical Geology, 2nd ed.: New York, McGraw-Hill, 686 p.

Moore, R. C., 1964, Paleoecological aspects of Kansas Pennsylvanian and Permian cyclothems, in Merriam, D. F., ed, Symposium on cyclic sedimentation: Lawrence, Kansas Geological Survey Bulletin 169, p. 287-380.

Muto, T., and Steel, R.J., 2004, Autogenic response of fluvial deltas to steady sea-level fall: Implications from flume-tank experiments: Geology, v. 32, p. 401–404.

Mutti, E., and Normark, W.R., 1987, Comparing examples of modern and ancient turbidite systems: problems and concepts, in Leggert, J.K., and Zuffa, G.G., eds., Marine Clastic Sedimentology; Concepts and Case Studies: London, Graham and Trotman, p. 1-38.

Northcutt, R.A., and Andrews, R.D., 1997, Fluvial-dominated deltaic (FDD) oil reservoirs in Oklahoma: The Bartlesville plays, Oklahoma Geological Survey Special Publication 97-6, 97 p.

Oakes, M.C., 1953, Krebs and Cabiness Groups, of Pennsylvanian Age, in Oklahoma: The Association of Petroleum Geologists Bulletin, v. 37, no. 6, p. 1523-1526.

Perry, Jr., W.J., 1989, Tectonic evolution of the Anadarko Basin region, Oklahoma: U.S. Geological Survey Bulletin 1866-A, 28p.

Potter, P.E., Maynard, J.B., and Depetris, P.J., 2005, Mud and Mudstones: Introduction and Overview: Berlin, Springer, 297 p.

Prothero, D.R., and Schwab, F.L., 2004, Sedimentary geology: An introduction to sedimentary rocks and stratigraphy (2nd ed.): New York: W.H. Freeman.

Puckette, J.O., 1990, Depositional setting, facies, and petrology of Cabaniss (Upper "Cherokee") Group in Beckham, Dewey, Custer, Ellis, Roger Mills, and Washita Counties, Oklahoma: unpublished Masters thesis, Okla. State University, 144 p.

Puckette, J.O., Anderson, C., and Al-Shaieb, S. 2000, The deep-marine Red Fork Sandstone: a submarine-fan complex, *in* Johnson, K. S. (ed.), Marine clastics in the southern Midcontinent, 1997 symposium: Oklahoma Geological Survey Circular 103, p. 177-184.

Rascoe, B., Jr., 1962, Regional stratigraphic analysis of Pennsylvanian and Permian rocks in western mid-continent, Colorado, Kansas, Oklahoma, Texas: American Association of Petroleum Geologists Bulletin, v. 46, p. 1345–1370.

Rascoe, B., Jr., and Adler, F.J., 1983, Permo-Carboniferous hydrocarbon accumulations, mid-continent USA: American Association of Petroleum Geologists Bulletin, v. 67, no. 6, p. 979-1001.

Rascoe, B., Jr., and Johnson, K.S., 1988, Anadarko basin and Hugoton embayment, in L. L. Sloss, ed., Sedimentary cover-North American craton: U.S.: the geology of North America: Boulder, Colorado, Geological Society of America, v. D-2, p. 318-326.

Reading, H.G. and M. Richards, 1994, Turbidite systems in deep-water basin margins classified by grain size and feeder system: AAPG Bulletin, v. 78, p. 792-822.

Rowe, H.D., Hughes, E.N., Robinson, R., 2012, The quantification and application of handheld energy-dispersive x-ray fluorescence (ED-XRF) in mudrock chemostratigraphy and geochemistry: Chemical Geology, vol. 324–325, p. 122-131.

Ross, C.A., and Ross, J.R.P.,1987, Late Paleozoic sea levels and depositional sequences, in C. A. Ross and D. Haman, eds., Timing and deposition of eustatic sequences: Constraints on seismic stratigraphy: Cushman Foundation for Foraminiferal Research Special Publication 24, p. 137-149.

Schieber, J., Southard, J.B., and Schimmelmann, A., 2010, Lenticular Shale Fabrics Resulting from Intermittent Erosion of Muddy Sediments-Comparing Observations

from Flume Experiments to the Rock Record: Journal of Sedimentary Research, v. 80, p. 119-128.

Schneider, R.E., and Clement, W.A., 1986, The East Clinton gas field, Custer County, Oklahoma: a seismicstratigraphic case history: Oklahoma City Geological Society, Shale Shaker Digest XII, p. 63-67.

Sinclair, H.D., 1992, Turbidite Sedimentation during Alpine thrusting: The Taveyannaz Sandstones of eastern Switzerland: Sedimentology, v. 39, p. 837-856.

Sinclair, H.D., 1997, Flysch to molasses transition in peripheral foreland basins: The role of the passive margin versus slab breakoff: Geology, v. 25, p. 1123-1126.

Sinclair, H.D. and Naylor, M., 2012, Foreland basin subsidence driven by topographic growth versus plate subduction: Geological Society America Bulletin, 124, p. 368–379.

Sloss, L.L., ed., 1988, Sedimentary cover—North American craton: U.S.: the geology of North America: Boulder, Colorado, Geological Society of America, v. D-2, 506 p.

Sorenson, R. P., 2005, A dynamic model for the Permian Panhandle and Hugoton fields, western Anadarko basin: American Association of Petroleum Geologists Bulletin, vol. 89, no. 7, p. 921-938.

Stanley, D. J., 1981, Unifites: Structureless muds of gravity-flow origin in Mediterranean basins: Geo-Mar. Lett., p. 77-84.

Stow, D.A.V., Bowen, A.J., 1978. Origin of lamination in deep-sea, fine-grained sediments: Nature, v. 274, p. 324-328.

Stow, D.A.V., Bowen, A.J., 1980. A physical model for the transport and sorting of fine-grained sediment by turbidity currents: Sedimentology 27, p. 31-46.

Stow, D.A.V., Cremer, M., Droz, L., Normark, W. R., O'Connell, S., et al., 1985. Mississippi Fan sediments: facies, composition and texture. In Bouma, A.H., Normark, W.R. and Barnes, N. E. (Eds.), Deep-Sea Fans and Related Turbidite Systems: New York (Springer-Verlag), p. 259-266.

Stow, D.A.V., Piper, D.J.W., 1984, Deep-water fine-grained sediments: facies models. In: Stow, D.A.V., Piper, D.J.W. (Eds.), Fine Grained Sediments: Deep-water Processes and Facies: Geol. Soc. London Spec. Publ. 15, p. 611-646.

Sweet, D.E., and Soreghan, G.S., 2008, Polygonal cracking in coarse clastics records cold temperatures in the equatorial Fountain Formation (Pennsylvanian-Permian, Colorado): Palaeogeography, Palaeoclimatology, Palaeoecology, v. 268.

Talling, P.J., Masson, D.G., Sumner, E.J., and Malgesini, G., 2012, Subaqueous sediment density flows: depositional processes and deposit types: Sedimentology, v. 59, p. 1937-2003.

Udayashankar, K.V., 1985, Depositional environment, petrology and diagenesis of Red Fork Sandstone in central Dewey County, Oklahoma: Oklahoma State University unpublished M.S. thesis, 188 p.

Van Dijk, M., Postma, G., and Kleinhans, M.G., 2009, Autocyclic behavior of fan deltas: an analogue experimental study: Sedimentology, v. 56, p. 1569-1589.

Veevers J.J., and Powell C.M., 1987, Late Paleozoic glacial episodes in Gondwanaland reflected in transgressive-regressive depositional sequences in Euramerica: Geological Society of America Bulletin, v. 98, p. 475–487.

Whiting, P.H., 1982, Depositional environment of Red Fork sandstones, deep Anadarko Basin, western Oklahoma: Oklahoma City Geological Society, Shale Shake Digest XI, p. 104-119.

Walker, R.G., 1978, Deep-water sandstone facies and ancient submarine fans-models for exploration and for stratigraphic traps: AAPG Bull., 62, p. 932–966.